

AD-A114 955

CHARLES STARK DRAPER LAB INC CAMBRIDGE MA

F/G 9/1

MATERIALS RESEARCH FOR ADVANCED INERTIAL INSTRUMENTATION: TASK --ETC(U)

DEC 81 D DAS, K KUMAR, E WETTSTEIN

N00014-77-C-0388

NL

UNCLASSIFIED

CSDL-R-1529

100  
1000

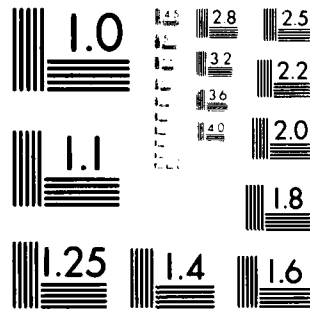
END

DATE

FILED

6 82

DTIC



MICROCOPY RESOLUTION TEST CHART  
NATIONAL BUREAU OF STANDARDS-1963-A

AD A114955

6-1000

**MATERIALS RESEARCH FOR ADVANCED  
INERTIAL INSTRUMENTATION**

**TASK 2. BASIC SCIENCE RESEARCH  
MATERIAL TECHNOLOGY AS RELATED TO  
GYRO TORQUES AND MOTORS**

**DECEMBER 1961**

**TECHNICAL REPORT NO. 1**

**1 OCTOBER 1960 - 30 SEPTEMBER 1961**

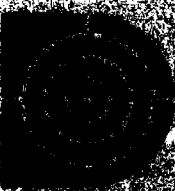
**By**

**D. DAS, K. KUMAR, E. WEITZBERG**

**Prepared for the Office of Naval Research, Department of the  
Navy, under contract N00017-60-0-1000**

**Approved for public release; distribution unlimited**

**Form Approved by GSA General Regulation 27 of the  
Federal Acquisition Regulation (41 CFR 101-11.6)**



**This document contains information of a classified nature  
and is to be controlled accordingly**

UNCLASSIFIED

SECURITY CLASSIFICATION OF THIS PAGE (When Data Entered)

| REPORT DOCUMENTATION PAGE   |                                      | READ INSTRUCTIONS<br>BEFORE COMPLETING FORM                                |                           |           |                |  |                                 |  |                        |                               |  |                     |                   |  |
|---|--------------------------------------|--|---------------------------|-----------|----------------|--|---------------------------------|--|------------------------|-------------------------------|--|---------------------|-------------------|--|
| 1. REPORT NUMBER<br>R-1529  | 2. GOVT ACCESSION NO.<br>AD-A114 953 | 3. RECIPIENT'S CATALOG NUMBER  |                           |           |                |  |                                 |  |                        |                               |  |                     |                   |  |
| 4. TITLE (and Subtitle)<br>Materials Research for Advanced Inertial Instrumentation; Task 3: Rare Earth Magnetic Material Technology as Related to Gyro Torquers and Motors   |                                      | 5. TYPE OF REPORT & PERIOD COVERED<br>Research Report<br>10/1/80 - 9/30/81 |                           |           |                |  |                                 |  |                        |                               |  |                     |                   |  |
| 7. AUTHOR(s)<br>D. Das, K. Kumar, and E. Wettstein  |                                      | 6. PERFORMING ORG. REPORT NUMBER   |                           |           |                |  |                                 |  |                        |                               |  |                     |                   |  |
| 9. PERFORMING ORGANIZATION NAME AND ADDRESS<br>The Charles Stark Draper Laboratory, Inc.<br>555 Technology Square<br>Cambridge, Massachusetts 02139   |                                      | 8. CONTRACT OR GRANT NUMBER(s)<br>N00014-77-C-0388                         |                           |           |                |  |                                 |  |                        |                               |  |                     |                   |  |
| 11. CONTROLLING OFFICE NAME AND ADDRESS<br>Office of Naval Research<br>Department of the Navy<br>800 N. Quincy St., Arlington, Virginia 20217   |                                      | 10. PROGRAM ELEMENT, PROJECT, TASK AREA & WORK UNIT NUMBERS                |                           |           |                |  |                                 |  |                        |                               |  |                     |                   |  |
| 14. MONITORING AGENCY NAME & ADDRESS (if different from Controlling Office)<br>Office of Naval Research<br>Boston Branch, Bldg. 114, Sec. D<br>666 Summer Street<br>Boston, Massachusetts 02210   |                                      | 12. REPORT DATE<br>December 1981   |                           |           |                |  |                                 |  |                        |                               |  |                     |                   |  |
|   |                                      | 13. NUMBER OF PAGES<br>71  |                           |           |                |  |                                 |  |                        |                               |  |                     |                   |  |
|   |                                      | 15. SECURITY CLASS. (of this report)<br>Unclassified                       |                           |           |                |  |                                 |  |                        |                               |  |                     |                   |  |
| 16. DISTRIBUTION STATEMENT (of this Report)<br><br>Approved for public release, distribution unlimited.   |                                      | 15a. DECLASSIFICATION/DOWNGRADING SCHEDULE                                 |                           |           |                |  |                                 |  |                        |                               |  |                     |                   |  |
| 17. DISTRIBUTION STATEMENT (of the abstract entered in Block 20, if different from Report)  |                                      |  |                           |           |                |  |                                 |  |                        |                               |  |                     |                   |  |
| 18. SUPPLEMENTARY NOTES   |                                      |  |                           |           |                |  |                                 |  |                        |                               |  |                     |                   |  |
| 19. KEY WORDS (Continue on reverse side if necessary and identify by block number)  |                                      |  |                           |           |                |  |                                 |  |                        |                               |  |                     |                   |  |
| <table border="0"> <tr> <td>SmCo<sub>5</sub> Magnets</td> <td>Sintering</td> <td>Flux Stability</td> </tr> <tr> <td>Sm<sub>2</sub>Co<sub>17</sub> Magnets</td> <td>Temperature Compensated Magnets</td> <td></td> </tr> <tr> <td>Hot Isostatic Pressing</td> <td>Thermal Expansion Coefficient</td> <td></td> </tr> <tr> <td>Arc Plasma Spraying</td> <td>Permanent Magnets</td> <td></td> </tr> </table> |                                      |  | SmCo <sub>5</sub> Magnets | Sintering | Flux Stability | Sm <sub>2</sub> Co <sub>17</sub> Magnets | Temperature Compensated Magnets |  | Hot Isostatic Pressing | Thermal Expansion Coefficient |  | Arc Plasma Spraying | Permanent Magnets |  |
| SmCo <sub>5</sub> Magnets   | Sintering                            | Flux Stability   |                           |           |                |  |                                 |  |                        |                               |  |                     |                   |  |
| Sm <sub>2</sub> Co <sub>17</sub> Magnets  | Temperature Compensated Magnets      |  |                           |           |                |  |                                 |  |                        |                               |  |                     |                   |  |
| Hot Isostatic Pressing  | Thermal Expansion Coefficient        |  |                           |           |                |  |                                 |  |                        |                               |  |                     |                   |  |
| Arc Plasma Spraying   | Permanent Magnets                    |  |                           |           |                |  |                                 |  |                        |                               |  |                     |                   |  |
| 20. ABSTRACT (Continue on reverse side if necessary and identify by block number)   |                                      |  |                           |           |                |  |                                 |  |                        |                               |  |                     |                   |  |
| <p>-Preliminary measurements of flux decay rates of high coercivity and high energy product hot isostatically pressed (HIPed) SmCo<sub>5</sub> magnets show that an increase of samarium content by one weight percent, increasing the Sm<sub>2</sub>Co<sub>7</sub> second phase, raises the decay rate from -43 ppm/decade to -1070 ppm/decade.</p> <p style="text-align: right;">(continued)</p>        |                                      |  |                           |           |                |  |                                 |  |                        |                               |  |                     |                   |  |

15/128 376

DD FORM 1473 EDITION OF 1 NOV 65 IS OBSOLETE  
1 JAN 73UNCLASSIFIED  
SECURITY CLASSIFICATION OF THIS PAGE (When Data Entered)

UNCLASSIFIED

SECURITY CLASSIFICATION OF THIS PAGE (When Data Entered)

This finding may prove to be extremely valuable for producing high stability  $\text{SmCo}_5$  magnets. Oxygen contamination, determined to be the other major cause of instability, is expected to be significantly lowered with the use of the facilities being developed for fabrication of oxygen-free  $\text{SmCo}_5$  magnets with the support of a related program.

Radially oriented full circle  $\text{SmCo}_5$  ring magnets have been impossible to produce by the sinter technology. Using the HIP technique, developed for  $\text{SmCo}_5$  magnets at CSDL, ring magnets of high magnetic properties with well controlled geometry have been produced. These are expected to play an important role in the magnetic circuitry of torque generators in inertial instruments.

Continued research in the area of temperature-compensated Re-Co magnets using HIP processing has resulted in substantial improvement of the remanence ( $B_r$ ). Zero-temperature-coefficient magnets of the ternary system Er-Sm-Co with a maximum energy product of nearly 15 MGOe appears feasible. Similar Tb-Sm-Co magnets appear to have a somewhat lower energy product potential of between 7 and 9 MGOe.

Additional deposits from starting powder compositions of 42.0, 34.5 and 28.3% Sm were fabricated using plasma spraying. X-ray diffraction patterns from the surfaces of these deposits showed a somewhat more crystalline material than was obtained earlier. Experiments performed at providing more cooling to the substrate with the use of liquid-nitrogen-chilled helium gas did not alter this situation. When these deposited materials were thermally treated for 16 hours in a hydrogen atmosphere the original as-sprayed x-ray peaks were found to disappear and new peaks representative of the hydride phase were found to develop. It was noted that the interaction of the deposit with the hydrogen gas was similar over this wide range of composition. These experiments also indicated a partial removal of the low level of as-sprayed crystallinity in the deposits in contradiction with some conclusions that were reached earlier. Experiments aimed at promoting texture in the deposits through thermal treatment in the presence of a magnetic field were initiated.

|                    |                                     |
|--------------------|-------------------------------------|
| Accession          |                                     |
| NTIS               | <input checked="" type="checkbox"/> |
| DTIC               | <input type="checkbox"/>            |
| Unannounced        | <input type="checkbox"/>            |
| Justification      |                                     |
| By                 |                                     |
| Distribution       |                                     |
| Availability Codes |                                     |
| Dist               | Avail and Special                   |
| A                  |                                     |



UNCLASSIFIED

SECURITY CLASSIFICATION OF THIS PAGE (When Data Entered)

R-1529

MATERIALS RESEARCH FOR ADVANCED INERTIAL INSTRUMENTATION

TASK 3: RARE EARTH MAGNETIC MATERIAL TECHNOLOGY  
AS RELATED TO GYRO TORQUERS AND MOTORS

DECEMBER 1981

TECHNICAL REPORT NO. 4

FOR THE PERIOD

October 1, 1980 to September 30, 1981

by

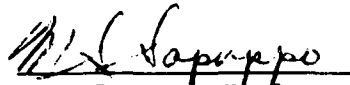
D. Das and K. Kumar,\* E. Wettstein

Prepared for the Office of Naval Research  
Department of the Navy, under Contract N00014-77-C-0388

Approved for Public Release; distribution unlimited

Permission is granted to the U.S. Government to reproduce this report in  
whole or in part.

Approved:



M.S. Sapuppo, Head  
Component Development Department

The Charles Stark Draper Laboratory  
Cambridge, Massachusetts 02139

\* Some of the work described in this report was performed at the  
Francis Bitter National Magnet Laboratory by the authors as visiting  
scientists.

#### ACKNOWLEDGEMENTS

We wish to express our appreciation to the National Magnet Laboratory, MIT, for their assistance by making their high-field magnets available for our studies in this program. Our sincere thanks to C.R. Dauwalter for carrying out the flux stability measurements.

This report was prepared by The Charles Stark Draper Laboratory, Inc., under Contract N00014-77-C-0388 with the Office of Naval Research of the Department of the Navy.

Publication of this report does not constitute approval by the U.S. Navy of the findings or conclusions contained herein. It is published for the exchange and stimulation of ideas.

## TABLE OF CONTENTS

| <u>Section</u>  | <u>Page</u> |
|---|-------------|
| 1. INTRODUCTION.....  | 1           |
| 1.1 Program Background.....   | 1           |
| 1.2 Objectives.....   | 2           |
| 2. SmCo <sub>5</sub> MAGNET INVESTIGATIONS.....                               | 3           |
| 2.1 Progress Prior to This Report.....  | 3           |
| 2.2 SmCo <sub>5</sub> Magnet Investigations During This Reporting Period..... | 5           |
| 2.2.1 Comminution and Encapsulation Chamber.....                              | 15          |
| 2.2.2 Radial Ring Magnet by HIP.....  | 17          |
| 2.2.3 Temperature Compensated Magnets.....                                    | 19          |
| 3. Sm-Co MAGNETS BY PLASMA SPRAYING.....                                      | 29          |
| 3.1 Objective.....  | 29          |
| 3.2 Background.....   | 29          |
| 3.3 Rationale for Adopted Approach.....                                       | 30          |
| 3.4 The Plasma Spray Process.....   | 31          |
| 3.5 Previous Work.....  | 32          |
| 3.6 Present Work.....   | 34          |
| 3.6.1 Deposit Fabrication.....  | 34          |
| 3.6.2 Effect of Low Temperature Treatments in Hydrogen.....                   | 34          |
| 3.6.3 Experiments on Annealing in a Magnetic Field.....                       | 43          |
| REFERENCES.....   | 55          |



# LIST OF FIGURES

| <u>Figure</u> |  | <u>Page</u> |
|---------------|--|-------------|
| 1             | Flux decay vs. log time for magnets H-26 and H-27.....   | 8           |
| 2             | Flux decay vs. log time for magnets H-28 and H-29.....   | 9           |
| 3             | Etched microstructure of H-26 following<br>62 hours at 950°C.....  | 11          |
| 4             | Etched microstructure of H-27 following<br>62 hours at 950°C.....  | 11          |
| 5             | Etched microstructure of H-28 following<br>62 hours at 950°C.....  | 12          |
| 6             | Etched microstructure of H-29 following<br>62 hours at 950°C.....  | 12          |
| 7             | Vacuum glove box schematic.....  | 16          |
| 8             | Macrophotograph of a radial magnet at a<br>magnification of approximately 1X of a<br>radial orientation $\text{SmCo}_5$ ring magnet<br>diffusion bonded to an inner iron ring..... | 20          |
| 9             | Microstructure of sintered Tb-Sm-Co magnet.....  | 23          |
| 10            | Microstructure of sintered Er-Sm-Co magnet.....  | 23          |
| 11            | Microstructure of sample No. H-4 in as-HIPed condition.....  | 26          |
| 12            | Microstructure of sample No. H-15 in as-HIPed condition.....   | 26          |
| 13            | Schematic sketch of spray process.....   | 31          |
| 14            | X-ray diffraction patterns on deposits formed from<br>(A) 42.0, (B) 34.5, and (C) 28.3% Sm<br>starting powder compositions.....  | 35          |
| 15            | X-ray diffraction patterns on deposits formed on<br>liquid nitrogen-chilled helium gas substrates.....   | 36          |
| 16            | X-ray patterns obtained on samples in Figure 15<br>after 550°C, 16-hour exposure in hydrogen.....  | 38          |
| 17            | X-ray patterns obtained on samples in Figure 17<br>after 550°C, 16-hour exposure in hydrogen.....  | 40          |
| 18            | Sample in Figure 17(A) showing expected "d" spacings<br>for the compound $\text{Sm}_2\text{O}_3$ .....   | 43          |
| 19            | Schematic sketch of modified furnace<br>used for magnetic annealing.....   | 45          |
| 20            | $4\pi\text{M}$ versus H behavior of as-sprayed deposit from<br>42.0% Sm powder.....  | 50          |
| 21            | $4\pi\text{M}$ versus H curves.....  | 51          |
| 22            | Demagnetization behavior after exposure:<br>1140°C, 2 hours + 900°C, 20 hours + quick cooling.....   | 52          |

# LIST OF TABLES

| <u>Table</u> |   | <u>Page</u> |
|--------------|---|-------------|
| 1            | Magnetic properties of 25 $\mu$ m-particle<br>magnets HIPed at 950°C.....   | 7           |
| 2            | Compositions of the temperature compensated<br>HIPed magnets.....   | 22          |
| 3            | Magnetic properties of HIPed temperature<br>compensated magnets.....  | 24          |
| 4            | X-ray data on 42.0, 34.5, and 28.3% Sm powder deposits<br>after the several indicated heat treatments.....                | 39          |
| 5            | X-ray data on 42.0% Sm powder deposit, obtained after<br>the heat treatments indicated.....                               | 42          |
| 6            | Magnetic properties of thermally treated<br>magnetically annealed Sm-Co deposits<br>without H <sub>2</sub> treatment..... | 47          |
| 7            | Magnetic properties of thermally treated deposits<br>magnetically annealed after H <sub>2</sub> treatment.....            | 48          |
| 8            | Magnetic properties of 42.0% Sm deposit<br>without magnetic alignment.....  | 49          |

## SECTION 1

### INTRODUCTION

#### 1.1 Program Background

Samarium-cobalt magnetic devices are used within inertial systems as components of the inertial instruments or sensors - the gyro and accelerometer - and as gimbal torque motors. As an example of the former category, samarium-cobalt permanent magnets are employed in the torque generator, or angular motion forcer, of the movable and buoyant member of the instrument. The torque generator is of cylindrical geometry, and in many designs the magnets are located on the moving member which must remain buoyant in fluid. Here the lower volume of Sm-Co magnets, because of their high energy product, impacts favorably on the overall size and weight of the completed instrument.

In addition to their high energy product, magnets utilized in precision inertial instruments must also possess excellent long-term flux stability, insensitivity to temperature change, and physical properties compatible with beryllium, which is the structural material of choice in modern inertial instruments.

A comprehensive program to develop samarium-cobalt magnets by powder-metallurgy techniques for these applications in future generations of inertial instruments was initiated at The Charles Stark Draper Laboratory (CSDL) in October 1977 under the sponsorship of the Office of Naval Research. During the first two years (October 1977 to September 1979) the efforts focused on sintered and hot isostatically pressed magnets of the  $\text{SmCo}_5$  composition. A new subtask was added as of October 1979 which concentrates on  $\text{Sm}_2\text{Co}_{17}$  magnets fabricated by the arc-plasma-spray process. The motivation behind this subtask was the earlier achievement of outstanding successes with  $\text{SmCo}_5$  magnets using this process at CSDL.

## 1.2 Objectives

The objectives of the present program are to investigate the arc-plasma-spray process for fabricating  $\text{Sm}_2\text{Co}_{17}$ -type magnets and to develop improved powder metallurgical procedures to produce inertial-grade  $\text{SmCo}_5$  magnets which would provide improvements in the following areas:

(1) Long-term flux stability at constant temperature ( $140^\circ\text{F}$ )

Desired: 0.008 ppm/90-day

Present capability: Sintered:  $\sim 1$  ppm/day

Plasma Sprayed: 0.05 ppm/day

(2) Thermal stability of residual induction

Desired: 0.1 ppm/ $^\circ\text{F}$

Present capability: 300 ppm/ $^\circ\text{F}$

(3) Tailoring of thermal expansion coefficient

Desired, same as beryllium: 6.6  $\mu\text{in./in. }^\circ\text{F}$

Isotropic: 4.7  $\mu\text{in./in. }^\circ\text{F}$

Anisotropic:

(a) Along magnetization direction: 3.1  $\mu\text{in./in. }^\circ\text{F}$

(b) Normal to magnetization direction: 7.1  $\mu\text{in./in. }^\circ\text{F}$

## SECTION 2

### SmCo<sub>5</sub> MAGNET INVESTIGATIONS

#### 2.1 Progress Prior to This Report

The objectives for this part of the magnetic materials program are: (1) high stability or low flux decay rate, (2) near-zero temperature coefficient of magnetic induction, and (3) tailored expansion coefficient to match that of beryllium.

Three interim annual reports<sup>(1,2,3)\*</sup> have been submitted, which described the progress in this area for a period of three years from October 1977 to September 1980. The highlights of the past performance are summarized below.

The most challenging of the three objectives was the achievement of a near-zero flux decay rate as compared to a decay rate of about 2000 ppm/decade of days in state-of-the-art SmCo<sub>5</sub> magnets. It was especially so because of a lack of adequate scientific understanding of the rather high decay rate of flux typically measured in these magnets. In contrast, the scientific basis for the other two objectives was quite clear,<sup>(4,5)</sup> and thus more easily obtainable than the first one. Efforts during the first two years were therefore devoted entirely to the first objective in order to achieve the objective as well as develop a scientific understanding of the phenomenon of flux decay in SmCo<sub>5</sub> magnets.

Since the decay of magnetic induction is a demagnetization process, higher stability would therefore demand a greater resistance to such a process. In turn this meant that both the intrinsic coercivity

---

\* Superscripted numerals refer to sources in the List of References.

$H_{ci}$  and  $H_k$  (reverse field at 90 percent  $4\pi M_R$ ) had to be improved substantially over the state-of-the-art magnets with  $H_{ci}$  in the range of 20 to 30 kOe and  $H_k$  of 5 to 10 kOe, notwithstanding the fact that these values were already an order of magnitude higher than those of the other permanent magnets known at the time. In order to achieve this difficult goal the  $SmCo_5$  magnet fabrication technique had to be improved to produce contamination-free magnets, particularly oxygen, with fine grain size. The standard sinter technology was consequently improved to produce magnets with outstanding intrinsic coercivity;  $H_{ci}$  of ~50 kOe and  $H_k$  of 33.5 kOe. This resulted in a flux decay rate of 280 ppm/decade. In a parallel effort, the hot isostatic pressing (HIP) technique was developed, for producing  $SmCo_5$  magnets which resulted in magnets with properties comparable to sintered magnets. The oxygen content of these magnets was about half of what is found in sintered magnets. Initial HIPed  $SmCo_5$  magnets showed an improved low decay rate of 160 ppm/decade.

At the beginning of the third year, experimental work was begun on the temperature compensated magnets as well as thermal expansion measurements, with the objectives of producing temperature stability and matching the expansion coefficient of the magnet with that of beryllium, in addition to the continued efforts on the study of flux stability. The investigations performed on temperature compensated magnets during the year consisted of experimental determination of compositions in the two ternary systems Er-Sm-Co and Tb-Sm-Co for zero temperature coefficient and the designing and building of an apparatus for rapid measurement of temperature coefficient of magnetic induction, with high precision. Based on published data on the variation of magnetic induction with temperature of the three binary compounds  $SmCo_5$ ,  $TbCo_5$  and  $ErCo_5$  the zero temperature coefficient in the systems Er-Sm-Co and Tb-Sm-Co should have occurred at 33.3 wt %  $ErCo_5$  + 66.7 wt %  $SmCo_5$  and 18.2 wt %  $TbCo_5$  + 81.8 wt %  $SmCo_5$  respectively. However, the preliminary experimental results from the measurements on die-pressed and sintered samples of various compositions in the two systems indicated that the zero temperature coefficients occurred at the compositions

40 weight percent  $\text{ErCo}_5$  and 40 weight percent  $\text{TbCo}_5$ . The higher amounts of the heavy rare earth compounds lower the magnetization values resulting in lower energy products. In addition, the measured magnetization values of the die-pressed and sintered samples were found to be about 25 percent smaller than the calculated values. This was attributed to poor alignment of the particles in the die-pressed and sintering process, most of which could be recovered by using cold isostatic pressing (CIP) of aligned powder and then HIP for the final densification.

The highest energy product CSDL  $\text{SmCo}_5$  magnets, prepared by HIP (21 MGOe) and die-pressed sintered (18 MGOe) were found to have 2 percent higher and 2 percent lower thermal expansion coefficients, respectively, than that of beryllium. Obviously an  $\text{SmCo}_5$  magnet with an energy product of between 19 and 20 MGOe would give a very satisfactory match with beryllium for thermal expansion compatibility, which would require little if any further effort. Temperature compensated magnets would, however, have to be measured for thermal expansion coefficient to determine the level of energy product at which the thermal expansion coefficient matches that of beryllium.

## 2.2 $\text{SmCo}_5$ Magnet Investigation During this Reporting Period

Prior studies had shown that the lowest flux decay rates obtained for magnets fabricated at Draper Laboratory were 280 ppm/decade of days for the sintered and 160 ppm/decade for the HIPed varieties. The sintered magnet had an average grain size of 20  $\mu\text{m}$ , although the starting powder particle size averaged 5 to 10  $\mu\text{m}$ . The HIPed sample, on the other hand, was prepared from a powder with an average particle size of 40  $\mu\text{m}$ , and retained the same grain size after the processing. The compositions were 36.5 weight percent samarium for the sintered magnet and 35.5 weight percent samarium in the case of the HIPed magnet. The samples were furnace cooled after the optimization annealing treatment at 900°C instead of the normal quick cooling. Furnace cooling was found to produce higher stability although the coercivities are lower than obtainable by quick cooling from the annealing temperature.

Since the coercivities of the tested sintered samples were higher than the tested HIPed samples in spite of the lower flux decay rates in the case of the HIPed samples, further investigation of the decay rates in various HIP samples were deemed necessary. The HIP samples H-26, H-27, H-28 and H-29 described in last year's report were picked for the present investigation. The intrinsic magnetic properties measured on these samples after various heat treatments are shown in Table 1, reproduced from last year's report. These had higher magnetic properties than the HIPed magnet tested before.

As described in earlier reports, the flux decay rate measurement apparatus requires 12 rectangular magnet samples of an identical geometry. These magnets are mounted on a C-49 alloy cylinder which in turn is introduced into a torque generator circuit and rotated at a constant speed for as long as the measurement continues. A voltage is generated in the pick-up coils. The decline of the voltage with time is a direct measure of the decay of the magnetic flux.

None of the samples H-26 through H-29 had enough material to produce a complete set of 12 flux measurement specimens for the intended decay rate measurements. There was, however, enough in each sample to produce at least half the required number. Therefore it was decided to combine six specimens each from H-26 and H-27 for one measurement and H-28 and H-29 combined for the other. Flux decay measurements were carried out on these two combination sets of samples, and as before the samples were heat treated at 1050°C for 24 hours, followed by 950°C for 24 hours followed by furnace cooling. The magnetic properties of the samples after the above treatment were expected to be the same as in the third row of Table 1. The resultant data from these measurements are shown in Figure 1 for the H-26 and H-27 specimens and Figure 2 for the H-28 and H-29 specimens. The flux decay when plotted against log time (in days) with zero time starting from the last heat treatment day gave a reasonably good linear relationship. The measurements in the past had shown the same behavior.



Table 1. Magnetic Properties of 25  $\mu\text{m}$ -particle magnets HIPed at 950°C.

| Thermal Treatment                         | Sample No. and Sm Content | H-26<br>35.5<br>wt % | H-27<br>36.0<br>wt % | H-28<br>36.5<br>wt % | H-29<br>37.0<br>wt % |
|---|---------------------------|----------------------|----------------------|----------------------|----------------------|
|   | Properties                |                      |                      |                      |                      |
| As-HIPed                                  | $B_r$ (kG)                | 8.9                  | 8.6                  | 8.6                  | 8.4                  |
|   | $H_{ci}$ (kOe)            | 20                   | 19                   | 18                   | 20                   |
|   | $H_k$ (kOe)               | 10                   | 10                   | 8                    | 7                    |
|   | $(BH)_{max}$ MGOe         | 20                   | 19                   | 17                   | 16                   |
| 950°C-62 h<br>Quick Cooled                | $B_r$ (kG)                | 9.2                  | 8.6                  | 8.7                  | 8.6                  |
|   | $H_{ci}$ (kOe)            | 36                   | 36                   | 34                   | 35                   |
|   | $H_k$ (kOe)               | 19                   | 14                   | 12                   | 10                   |
|   | $(BH)_{max}$ MGOe         | 21                   | 18                   | 18                   | 18                   |
| As Above<br>Furnace<br>Cooled             | $B_r$ (kG)                | 9.1                  | 8.7                  | 8.9                  | 8.7                  |
|   | $H_{ci}$ (kOe)            | 18                   | 26                   | 29                   | 31                   |
|   | $H_k$ (kOe)               | 6.5                  | 8.0                  | 7.5                  | 8.5                  |
|   | $(BH)_{max}$ MGOe         | 18                   | 17                   | 17                   | 17                   |
| 1050°C-24 h<br>900°C-24 h<br>Quick Cooled | $B_r$ (kG)                | 9                    | 8.5                  | 8.7                  | 8.6                  |
|   | $H_{ci}$ (kOe)            | 33                   | 35.5                 | 33.5                 | 33.5                 |
|   | $H_k$ (kOe)               | 26                   | 20                   | 17.5                 | 18                   |
|   | $(BH)_{max}$ MGOe         | 20                   | 20                   | 18                   | 18                   |

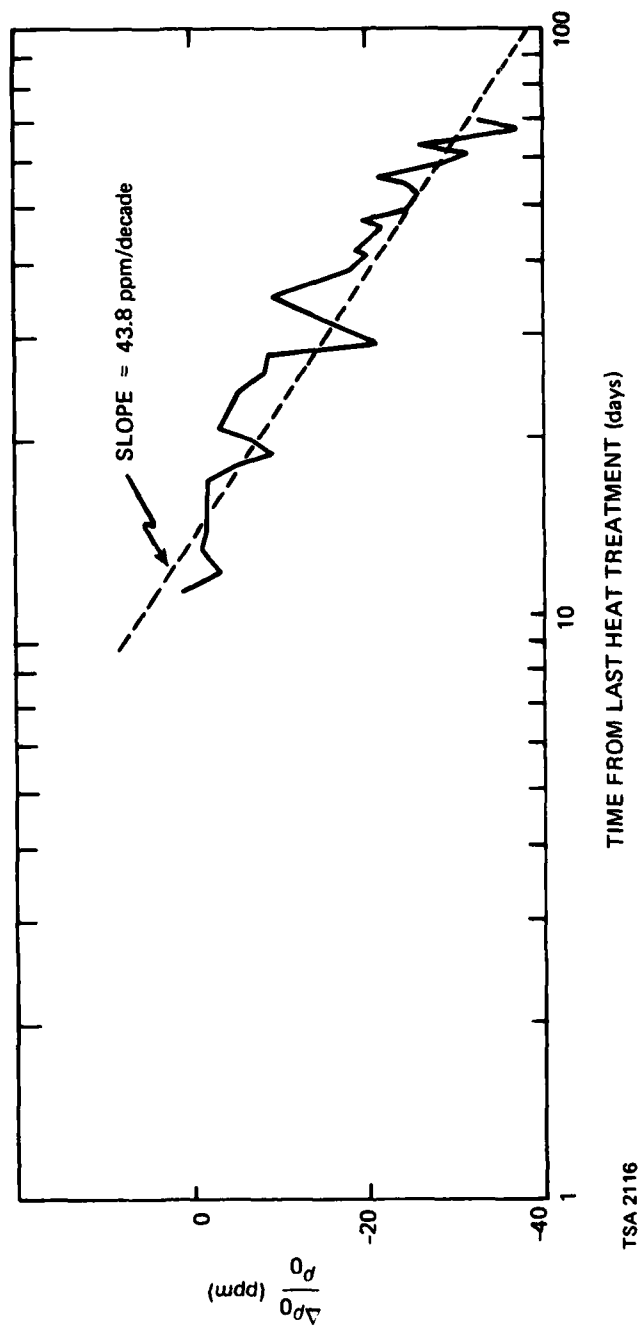


Figure 1. Flux decay vs. log time for magnets H-26 and H-27.

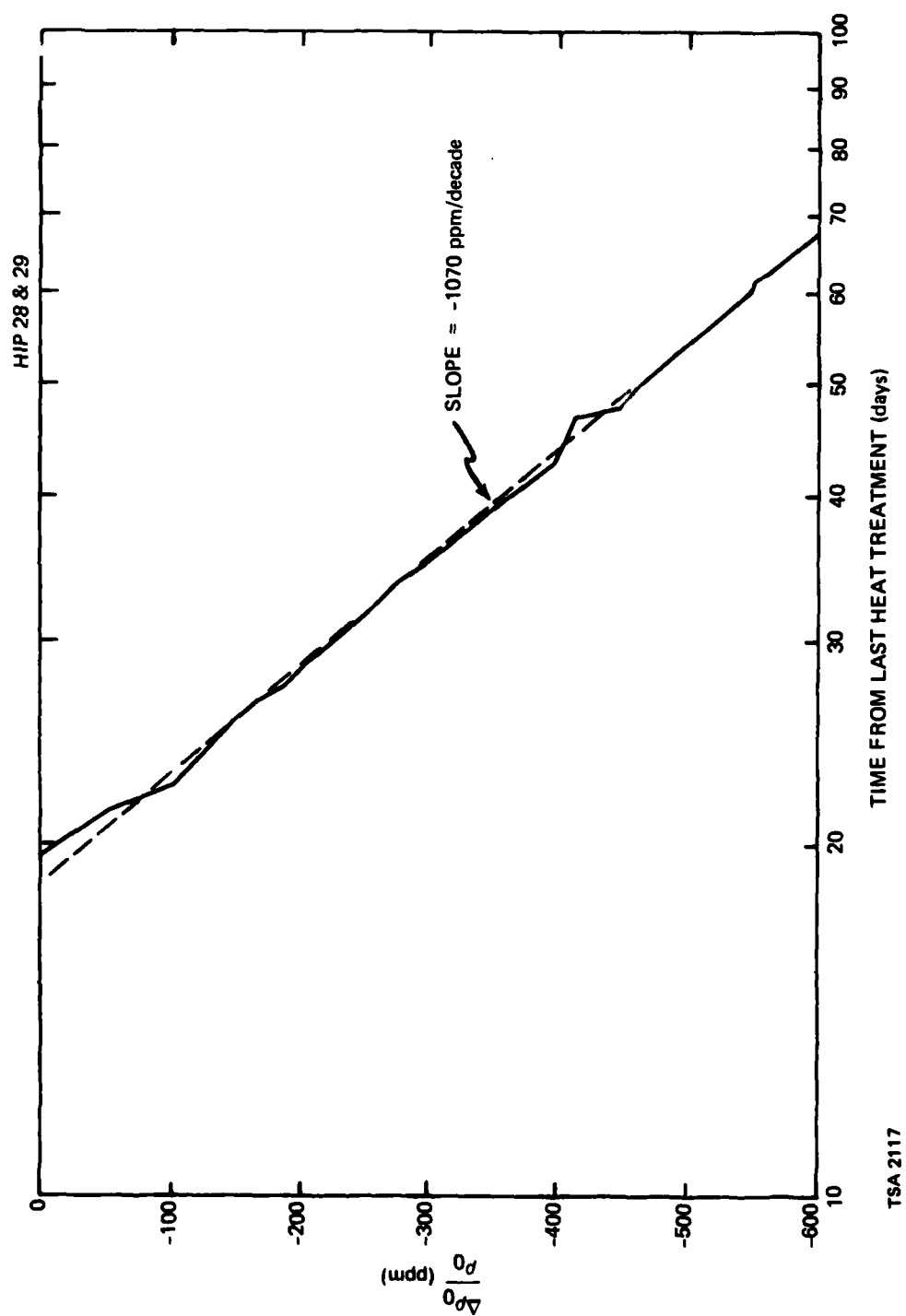
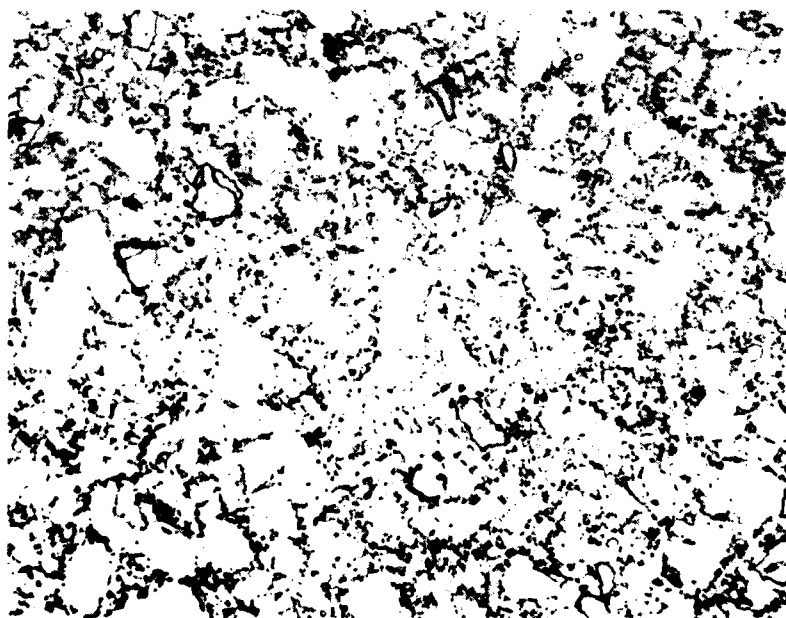


Figure 2. Flux decay vs. log time for magnets H-28 and H-29.

The decay rates obtained from Figures 1 and 2 are a low 43.8 ppm/decade for the set comprised of H-26 and H-27 magnets and a very high 1070 ppm/decade for the H-28 and H-29 set. This would appear to be a contradiction of our previous contention that an  $\text{SmCo}_5$  magnet that shows lesser degradation of coercivity on slow cooling from annealing temperature should also have a lower flux decay rate. The magnets H-28 and H-29 showed lesser degradation of coercivity than the H-26 and H-27 magnets (see rows 1 and 2 in Table 1), and therefore should have shown smaller decay rate than the set comprised of H-26 and H-27 on that basis but gave exactly the opposite of what was expected. However, a closer study of the rest of the facts known about these magnets provides a quite plausible explanation of this seeming contradiction. If the explanation is correct then it would not only result in a greatly broadened understanding of the mechanism of flux decay in the  $\text{SmCo}_5$  magnets; it will also perhaps show us the way to approach the extremely ambitious goal of producing near-zero decay rates in  $\text{SmCo}_5$  magnets.

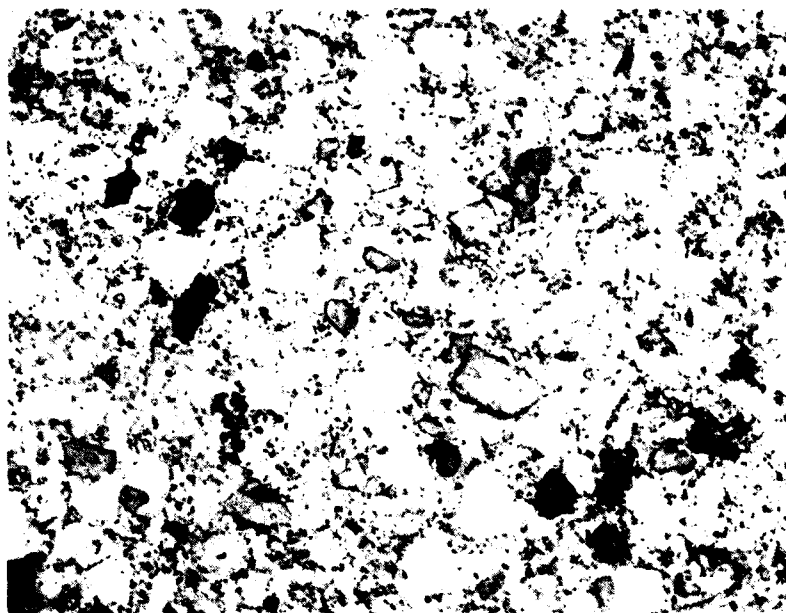
Figures 3 through 6 are typical micrographs of the samples H-26 through H-29, after the HIPed samples were homogenized at 950°C for 62 hours. The metallographically polished samples were etched with 3 percent nital solution, which produces a contrast between the  $\text{SmCo}_5$  (light) and  $\text{Sm}_2\text{Co}_7$  (dark) grains.

The micrographs clearly show that the least and the largest amounts of the second phase ( $\text{Sm}_2\text{Co}_7$  in this case) occur in the samples H-26 and H-29 with gradually increasing amounts going from H-26 through H-29. This is a qualitative confirmation of the compositions of those HIPed magnets shown in Table 1. It can therefore be realized that of the two sets of flux stability specimens, the set comprised of H-26 and H-27 had a lot less  $\text{Sm}_2\text{Co}_7$  than the H-28 and H-29 set. This was the only significant difference between these two sets of specimens, while the other relevant characteristics, such as grain size, oxygen content and thermal history, were as identical as possible. Therefore, in the case of these two sets of samples, it appears that the amounts of the



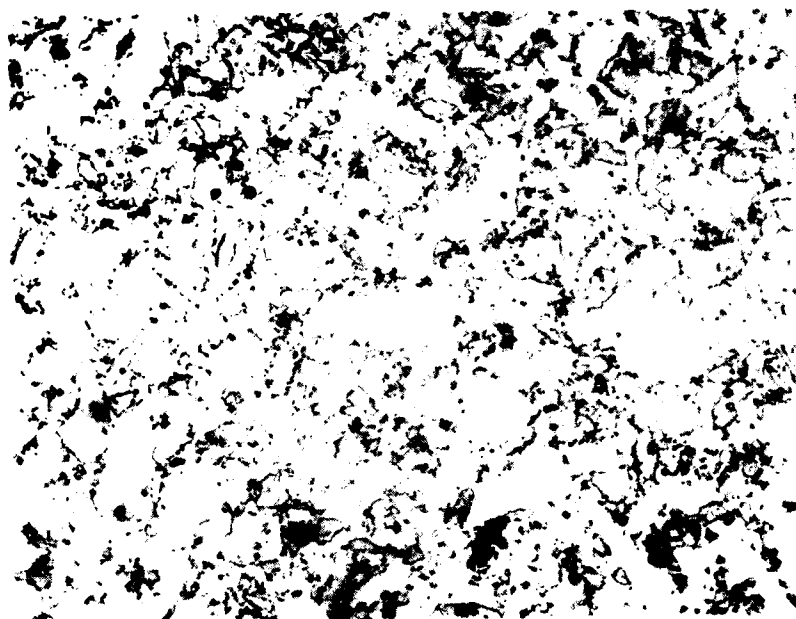
TSA 2118

Figure 3. Etched microstructure of H-26 following 62 hours at 950°C. 500x



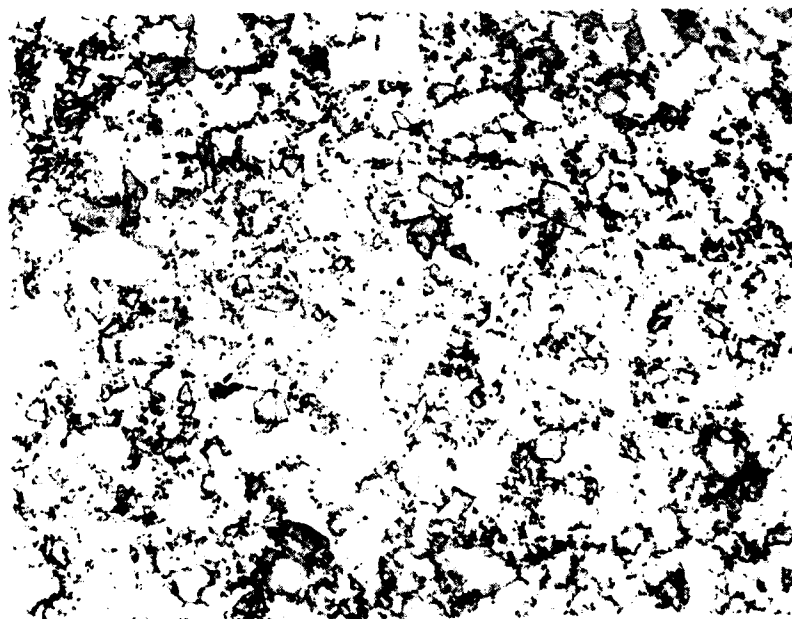
TSA 2119

Figure 4. Etched microstructure of H-27 following 62 hours at 950°C. 500x



TSA 2121

Figure 6. Etched microstructure of H-29 following 62 hours at 950°C. 500x



TSA 2120

Figure 5. Etched microstructure of H-28 following 62 hours at 950°C. 500x

second phase  $\text{Sm}_2\text{Co}_7$  had a great influence on the flux stability, and that the larger amounts of this phase caused greater deterioration of the stability. The data base for the conclusion is admittedly quite small and requires more confirming evidence. Nevertheless, the damaging effect of the second phase  $\text{Sm}_2\text{Co}_7$  does have a reasonable explanation. The compound  $\text{Sm}_2\text{Co}_7$  is a ferromagnetic material like  $\text{SmCo}_5$ . But the anisotropy field is only about 40 kOe, which is significantly lower than 350 kOe for  $\text{SmCo}_5$ . It is reasonable to conclude that demagnetization would occur in the  $\text{Sm}_2\text{Co}_7$  grains in an  $\text{SmCo}_5$  magnet at a comparatively low reverse magnetic field, provided by the self demagnetization of the magnet itself. Such a reverse field, of course, would not be large enough to reverse an  $\text{SmCo}_5$  grain free of defects. If the reasoning is valid, then the larger the amount of  $\text{Sm}_2\text{Co}_7$  phase the larger would be the flux decay rate. In order to verify the conclusion and quantify the relationship between the amount of  $\text{Sm}_2\text{Co}_7$  and the flux decay rate further experimental determinations are necessary and they will be carried out in our continuing efforts in this research program.

Based on the present investigations and the findings described in our previous reports, it appears that there are two identified mechanisms which are the major causes of decay of flux in the  $\text{SmCo}_5$  magnets:

- (1) Presence of  $\text{Sm}_2\text{Co}_7$  in the magnet body because of the composition of the alloy used in the fabrication of the magnet by sintering
- (2) Formation of  $\text{Sm}_2\text{Co}_{17}$  caused by the precipitation of dissolved oxygen in the  $\text{SmCo}_5$  lattice

In the prevailing conventional process for manufacturing of commercial fine-particle  $\text{SmCo}_5$  magnets, the final densification is obtained by the sintering of the powder compacts. It has been found essential to have the element samarium in excess of the  $\text{SmCo}_5$  stoichiometry, in order to produce sufficient densification at a reasonably low sintering temperature. The excess samarium used appears in the sintered magnet as the second phase  $\text{Sm}_2\text{Co}_7$ . Therefore the very process that is used to fabricate these commercially available magnets does by necessity introduce a built-in mechanism for the decay of flux with time. It can be reduced to a certain minimum value, but would still remain unacceptably high for our purpose. The above difficulty with the sintering process can be avoided by the use of the HIP process developed at Draper Laboratory for the fabrication of  $\text{SmCo}_5$  magnets under the present contract. Using this process the excess  $\text{Sm}_2\text{Co}_7$  can be entirely eliminated from the composition of the alloy, since the densification occurs by applied external pressure rather than by the enhanced diffusion achieved by the controlled chemical composition of the alloy powder.

The other major cause of the decay of flux in  $\text{SmCo}_5$  magnets, as brought out in our previous reports, is the unavoidable contamination of the alloy powder by oxygen from the air during powder preparation and handling of the powder. Since larger particle size powder can be used in the HIP technique than in the sinter process, it has been possible to reduce the oxygen content to about 0.3 weight percent in HIPed magnets as compared to 0.6 weight percent or even higher in the sintered variety. The result has been an improved flux stability. However, although further reduction of the oxygen content is desirable, present powder preparation and handling methods are not capable of doing it. In a related  $\text{SmCo}_5$  magnet program funded by NASA a powder preparation and encapsulation chamber has been designed and is now being built by an independent vendor, which will help to produce HIPed magnets with significantly lowered oxygen content. Since the use of this chamber is expected to contribute to the continuing ONR supported program, a description of the chamber is presented in the following section.

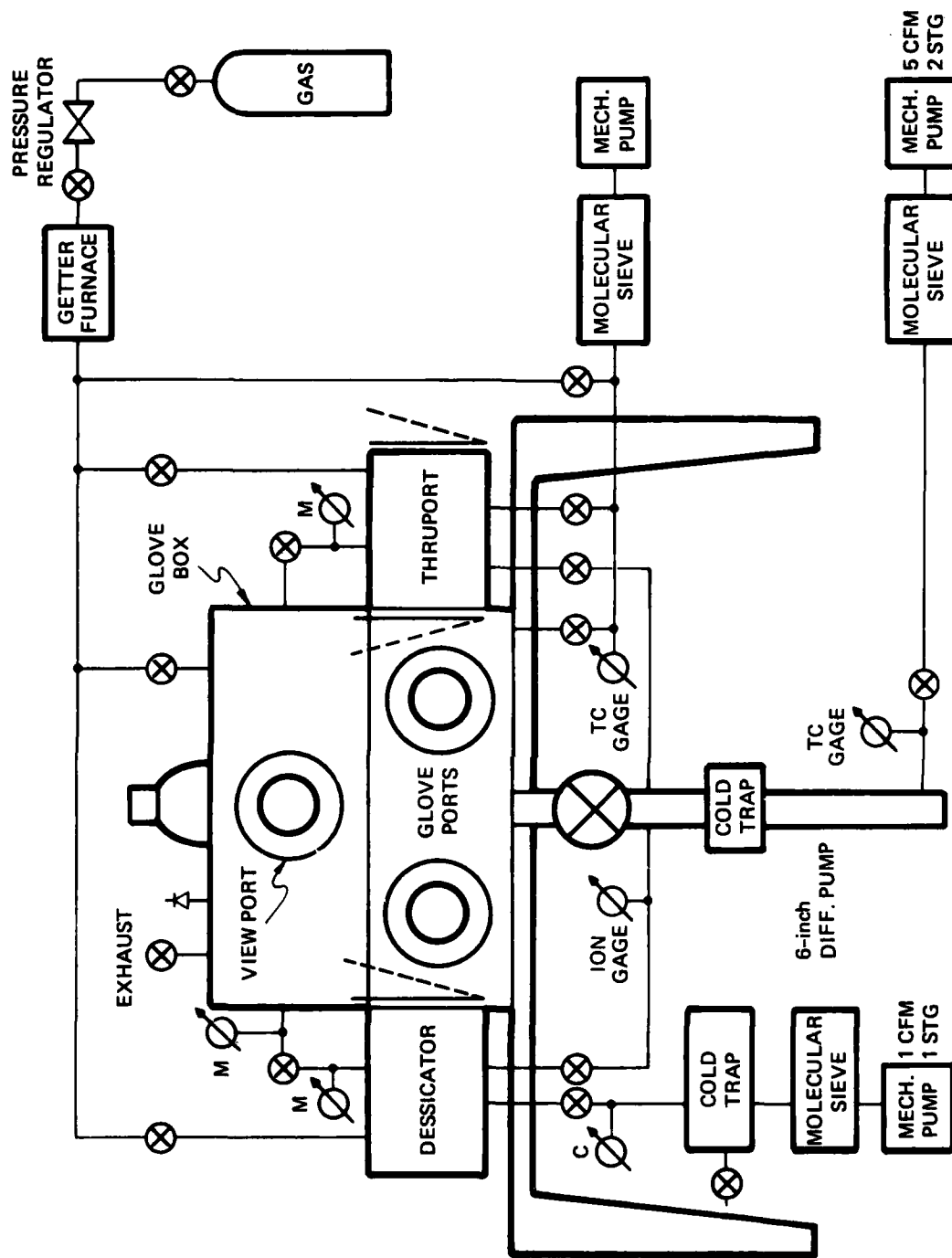


### 2.2.1 Comminution and Encapsulation Chamber

A large amount of oxygen (as much as 6000 ppm) is absorbed by the alloy powder of average 10- $\mu$ m particle size upon exposure to air. In the standard procedure, comminution and all powder handling is performed in air, until the green compacts enter the sintering furnace. Under very carefully controlled conditions, sintering can be performed without any large increase in oxygen content. At Draper Laboratory we have developed HIP for  $\text{SmCo}_5$  magnets, which is superior to sintering in lowering oxygen pickup during the densification of the powder compact.

The major problems that need to be solved are the preparation of powder from the  $\text{SmCo}_5$  alloy without exposure to any oxygen source and introduction of the powder into a well-outgassed HIP cannister, followed by evacuation and sealing of the cannister. All of the above steps can be performed inside a chamber filled with ultra-pure noble gas. Such a chamber has been designed and is now being built at a local vendor's place. A schematic sketch of the entire system is shown in Figure 7.

The chamber, being built of stainless steel with polished walls and stainless steel plumbing, will be capable of being evacuated and baked out to reach a low  $10^{-6}$ -torr pressure. Besides the main chamber where all the powder preparation and handling etc. will be performed using gloves, there will be two attached auxiliary chambers, one for powder drying and the other an entry port. After evacuation the chamber will be filled with Getter furnace purified argon to atmospheric pressure. The final comminution of the powder will be carried out inside the chamber, dried in the attached desiccator, loaded into the HIP cannister and compacted at 2000 lb/in<sup>2</sup>. The HIP canister will then be sealed by welding before being brought out for HIPing.



TSA 2122

Figure 7. Vacuum glove box schematic.

Using the procedure outlined above, it should be possible to maintain an oxygen level in the densified magnet at less than an order of magnitude smaller than is possible now. Initially the magnets produced will be isotropic and thus of low energy product. However, if oxygen content can be maintained at the desired low level, coils will be designed, built and installed inside the chamber to apply pulsed magnetic field of high intensity for aligning the powder particles during compaction to produce high energy product magnets.

#### 2.2.2 Radial Ring Magnet by HIP

In many applications such as inertial instruments, motors, generators, magnetic bearings, various microwave oscillators and amplifiers, etc., radially oriented  $\text{SmCo}_5$  ring magnets would be extremely useful. In spite of a great deal of effort to produce them by the conventional sintering process, there has been no success. Limited success was achieved a few years ago <sup>(6)</sup> using the hot pressing technique. But because of many disadvantages associated with the process, the method has not become a commercial process.

In the absence of a radially oriented ring magnet, the magnet design engineers are adapting any of the following compromises as a substitute, which at best are inferior in performance and are generally more expensive.

- (1) Randomly oriented (isotropic) magnets can be radially magnetized. The  $(BH)_{\text{max}}$  in these magnets is only a fourth of the theoretical maximum. The magnetic field strength is therefore drastically reduced.

- (2) In some cases, a large number of parallel line oriented magnets are assembled along the circumference of a circle, which gives an approximation to radial orientation. The larger the number of magnets used, the closer it gets to true radial orientation. Since the fabrication process is highly labor intensive the resultant cost of this format is high. There is, of course, some distortion in the geometry of the field. By using very large numbers of magnets the distortion can be minimized, but not eliminated.
- (3) Arc segments with small included angles and good radial orientation can be produced by conventional sintering process. However, they tend to lose their geometry during sintering. Besides this too is a labor intensive fabrication process and therefore expensive.
- (4) Recently radial arc segment of up to 114 deg included angle, with lengths of up to about 2 inches and thin walls have been produced by die pressing and sintering techniques.<sup>(7)</sup> It does not appear that this method is capable of producing full circle geometry of diffusion bonded supporting structures which serve as part of the overall circuit.

HIP processing for the Sm-Co magnets developed at the Draper Laboratory during the past few years under the ONR contract appeared to have the potential for successful production of radially oriented full circle magnets. Outstanding success has resulted in the development of HIP fabrication of radial ring magnets.

During the HIPing cycle, a diffusion bond is formed at the interface between the RE-Co alloy rings and the iron at both the ID and OD of the magnet cylinder. In some applications, it may be desirable to produce such a bonded structure. Where such a bonded structure is not desired, the bonding can be prevented by placing a barrier layer of thin tantalum foil between the magnet alloy compact and the HIPing canister.

When the iron canister is removed from the HIPed sample by acid solution, the reaction ceases when the acid reaches the tantalum foil. The foil can then be peeled off from the magnet,<sup>(8)</sup> because of the lack of bonding between the foil and the magnet alloy.

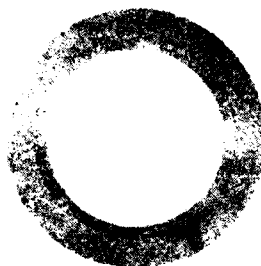
In our first attempt at the fabrication of radial ring geometries by HIP, we produced a large number of 1/4-inch-high magnet rings with OD = 1-7/16 inches and ID = 1-1/16 inches diffusion bonded to an iron ring of 1/16-inch wall thickness. A macrophotograph of such a ring is shown in Figure 8.

Although not visible in the macrophotograph, there are some radial cracks in the  $\text{SmCo}_5$  layer. These cracks are believed to have occurred during the cooling cycle in the HIP operation. The cracking is expected to be eliminated in future similar HIP operations by improved material selection and processing procedures.

For magnetic measurements, a number of 0.2-inch-diameter x 1/16-inch-high discs were machined from the  $\text{SmCo}_5$  layer of the radial cylinder from random locations, in such a manner, that the flats on the discs were parallel to the tangential plane of the cylinder. These measurements showed measured parameter to be within 1 percent of the average value. The average values are:  $B_r$ -8.8 kG,  $H_{ci}$ -28.0 kOe,  $H_k$ -21.0 kOe,  $H_c$ -8.6 kOe,  $(BH)_{\max}$ -18.9 MGOe. Because of the radial orientation, the true values of  $B_r$  and  $(BH)_{\max}$  would be somewhat higher in the radial direction than the measured value.

### 2.2.3 Temperature Compensated Magnets

At the operating temperature of inertial instruments, in the temperature range of 140° to 160°F, the  $\text{SmCo}_5$  magnets used in their sensor circuitry should possess near-zero temperature coefficient. The published values of temperature coefficient for  $\text{SmCo}_5$  magnets, by various manufacturers indicate that it is somewhere around 300 ppm/°F for the temperature range of room temperature to about 400°F.



TSA 2123

Figure 8. Macrophotograph of a radial magnet at a magnification of approximately 1× of a radial orientation  $\text{SmCo}_5$  ring magnet diffusion bonded to an inner iron ring.

The coefficient, however, becomes larger at higher temperatures. For the small range of temperature for gyro operations the coefficient is a constant for all intent and purpose. Recent measurements at CSDL on high energy product HIPed  $\text{SmCo}_5$  magnets have shown that the coefficient is about 180 ppm/°F in the temperature range of 130° to 160°F.

Most heavy rare earth-cobalt compounds show positive temperature coefficients in the temperature range of interest as opposed to the negative coefficient for  $\text{SmCo}_5$ . The two very promising compounds are  $\text{ErCo}_5$  and  $\text{TbCo}_5$ , with positive coefficients of nearly 2 times and 4.5 times respectively of that of the negative value of  $\text{SmCo}_5$ . Calculations showed that magnets of compositions 66.7 wt %  $\text{SmCo}_5$  + 33.3 wt %  $\text{ErCo}_5$  and 18.2 wt %  $\text{TbCo}_5$  + 81.8 wt %  $\text{SmCo}_5$  should have near-zero temperature coefficients at gyro operating temperatures. Our initial experiments to determine the compositions using die-pressed and sintered magnets gave results indicating that the zero coefficient in the two systems occurred at 60 wt %  $\text{SmCo}_5$  + 40 wt %  $\text{ErCo}_5$  and 60 wt %  $\text{SmCo}_5$  + 40 wt %  $\text{TbCo}_5$ . The theoretical value of residual induction ( $B_r$ ) of the above two compositions are 8 kG 7.1 kG with the potential maximum energy products ( $\text{BH}_{\text{max}}$ ) of 16 and 12.6 MGOe, respectively. The initial sintered samples of above compositions had  $B_r$  and ( $\text{BH}$ )<sub>max</sub> of 5.4 kG and 7.1 MGOe for the  $\text{ErCo}_5$  +  $\text{SmCo}_5$  alloy. The  $H_{ci}$  values were 20 to 30 kOe, which were high enough so that if the  $B_r$  values could be increased, the ( $\text{BH}$ )<sub>max</sub> values would also tend to approach the theoretical potential. Die-pressed sintered magnets tend to be poorly aligned, which causes the  $B_r$  values to be low. When the alloy powder is magnetically aligned and cold isostatically compacted followed by densification by HIPing, there is usually a substantial improvement in the  $B_r$  values.

It was therefore decided that a batch of temperature compensated magnets be fabricated by HIP technique. In the preliminary sintered samples, the compositions were adjusted to maintain a rare earth to cobalt ratio the same as in a 36.5 wt % Sm + 63.5 wt % Co alloy by the addition of a calculated amount of a 41.8 wt % Sm + 58.2 wt % Co alloy to a mixture of the  $\text{ErCo}_5$  or  $\text{TbCo}_5$  plus  $\text{SmCo}_5$  alloy powders. The

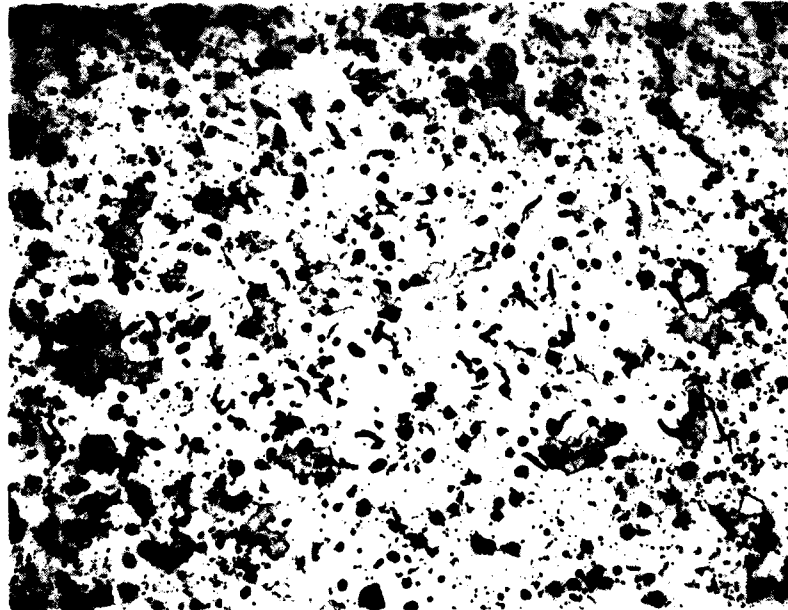
amounts of the three alloys were so adjusted that a predetermined ratio of Sm to Er or Sm to Tb was achieved in the final mixture. Although the coercivities in these preliminary samples were excellent, the microstructures showed excessive amounts of the  $RE_2Co_7$  phase. Figure 9 is a representative microstructure of a Tb-Sm-Co sintered magnet with Tb to samarium ratio of 23 to 77 and Figure 10 is that of a Er-Sm-Co magnet with Er to samarium of 33 to 67. The matrix is the 1-5 compound and the darker second phase is the 2-7 compound. The amounts of 2-7 second phase appears to be too high in both cases.

Since the amount of 1-7 type second phase was seen to be too high, the amount of samarium-rich additive was reduced in the mixtures for HIP fabrication. Table 2 shows the compositions used.

Table 2. Compositions of the temperature compensated HIPed magnets.

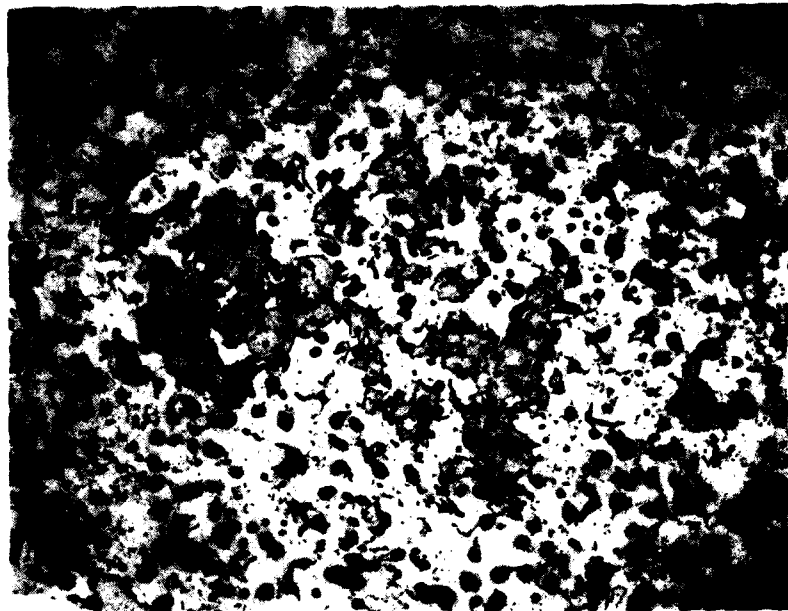
| Sample No. | Ternary System | R.E. (%) | TbCo <sub>5</sub> (%) | Sample (%) | Ternary System | R.E. (%) | ErCo <sub>5</sub> (%) |
|------------|----------------|----------|-----------------------|------------|----------------|----------|-----------------------|
| H-1        | Tb-Sm-Co       | 36.0     | 45                    | H-9        | Er-Sm-Co       | 36.0     | 45                    |
| H-2        | "              | "        | 40                    | H-10       | "              | "        | 40                    |
| H-3        | "              | "        | 35                    | H-11       | "              | "        | 35                    |
| H-4        | "              | "        | 30                    | H-12       | "              | "        | 30                    |
| H-5        | "              | 35.5     | 45                    | H-13       | "              | 35.5     | 40                    |
| H-6        | "              | "        | 40                    | H-14       | "              | "        | 35                    |
| H-7        | "              | "        | 35                    | H-15       | "              | "        | 30                    |
| H-8        | "              | "        | 30                    |            |                |          |                       |





TSA 2124

Figure 9. Microstructure of sintered  
Tb-Sm-Co magnet.  
Tb/Sm = 23/77. 200×



TSA 2125

Figure 10. Microstructure of sintered  
Er-Sm-Co magnet.  
Er/Sm = 33/67. 200×

The various powder mixtures of Table 2 were blended, aligned inside a rubber cylinder and CIPed to form cylindrical compacts 5/8 inch in diameter and 1-1/2 inches long. The 15 cylinders were then loaded into 5 HIP canisters of 1020 steel, evacuated, baked out, sealed and HIPed at 950°C under 15 kpsi of argon for 2 hours. The three samples in each canister were kept separated from each other by means of thin discs of stainless steel. Out of the five HIP canisters, four HIPed well and one containing sample numbers 7, 8 and 9 failed because of micro-leaks in a welded joint on the canister. The samples were removed from the canister by dissolving the iron can in nitric acid. The cylindrical HIPed magnets were sliced to produce 0.2-inch-thick discs for thermal treatments, and measurements of both intrinsic magnetic properties and temperature coefficients. The results of these measurements are shown in Table 3.

Table 3. Magnetic properties of HIPed temperature compensated magnets.

| Sample<br>No. | As HIPed            |                       | Thermally Treated-1050° for 71 hrs.<br>900°C for 24 hrs., Quick Cooled |                       |                                 |                     | Temp. Coeff.<br>of B (130°-160°F)<br>(PPM/°F) |
|---------------|---------------------|-----------------------|--|-----------------------|---------------------------------|---------------------|---|
|               |                     |                       | B <sub>r</sub> (kG)  | H <sub>ci</sub> (kOe) | (BH) <sub>max</sub><br>Measured | (MGOe)<br>Potential |   |
|               | B <sub>r</sub> (kG) | H <sub>ci</sub> (kOe) |  |                       |                                 |                     |   |
| H-1           | 5.0                 | 4.5                   | 5.1  | 21.0                  | 5.9                             | 6.5                 | +30   |
| H-2           | 5.6                 | 5.3                   | 5.4  | 19.0                  | 5.9                             | 7.3                 | +10   |
| H-3           | 5.5                 | 2.5                   | 5.4  | 2.5                   | 2.4                             | 7.3                 |   |
| H-4           | 6.2                 | 7.0                   | 6.2  | 28.0                  | 9.3                             | 9.6                 | -30   |
| H-5           | 5.0                 | 3.1                   | 4.9  | 6.0                   | 3.8                             | 6.0                 |   |
| H-6           | 5.4                 | 3.2                   | 5.4  | 3.0                   | 3.0                             | 7.3                 |   |
| H-10          | 6.7                 | 1.7                   | 7.3  | 2.8                   | 3.7                             | 13.3                |   |
| H-11          | 7.2                 | 2.0                   | 7.7  | 12.5                  | 8.7                             | 14.8                | -20   |
| H-12          | 7.4                 | 1.7                   | 7.8  | 1.2                   | 2.6                             | 15.2                |   |
| H-13          | 6.7                 | 1.0                   | 7.0  | 1.2                   | 1.8                             | 12.3                |   |
| H-14          | 7.0                 | 1.5                   | 7.8  | 2.0                   | -                               | 15.2                |   |
| H-15          | 7.5                 | 1.2                   | 8.0  | 1.0                   | 2.4                             | 16.0                |   |

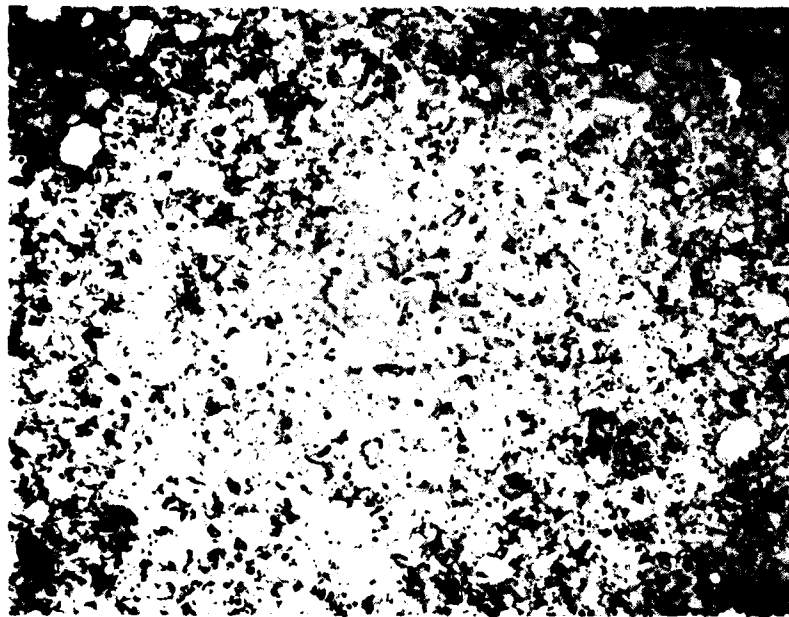
In as-HIPed condition, the coercivities were low for all the compositions. Of the various thermal treatments tried, the one that gave the best results in improving the coercivity is shown in Table 3. A few samples such as H-1, H-2, H-4 showed good coercivities after the treatment and H-11 gave some improvement, although not quite good enough. The reason for the low coercivities in these HIPed magnets can be seen in the microstructures. Figure 11 shows a typical microstructure of Sample H-4. A few isolated grains of  $\text{Sm}_2\text{Co}_{17}$  (very light particles) and a few isolated grains of  $\text{Sm}_2\text{Co}_7$  (dark gray) can be seen in a light gray matrix of  $\text{SmCo}_5$ . In this nonequilibrium state, the  $H_{ci}$  value was 7 kOe. After the long-time anneal of 70 hours at  $1050^\circ\text{C}$ , a single-phase  $\text{SmCo}_5$  equilibrium structure would result, and as a result the  $H_{ci}$  value went up to a reasonably high value of 28 kOe. In contrast the microstructure of sample No. H-15 shows a high amount of  $\text{Sm}_2\text{Co}_{17}$  (Figure 12), which caused the  $H_{ci}$  to be only 1.2 kOe. Also to be noted is that there are not enough  $\text{Sm}_2\text{Co}_7$  grains to convert all the  $\text{Sm}_2\text{Co}_{17}$  to  $\text{SmCo}_5$ . The long-time anneal therefore resulted in no improvement of the coercivity. All the samples showed similar presence of  $\text{Sm}_2\text{Co}_{17}$  indicating that the rare earth content in these compositions was either marginal or too low. This can be corrected by increasing the ratio of rare earth to cobalt in future temperature compensated magnets.

The main purpose of fabricating these HIPed magnets was to try to improve the  $B_r$  values over what was obtained in the die-pressed and sintered magnets of these temperature compensated compositions. This has been accomplished. The Erbium-based compositions between 30 and 40 percent  $\text{ErCo}_5$  of the total  $\text{RECo}_5$  give an average  $B_r$  of 7.6 kG compared to 5.4 kG in the same range of compositions of die-pressed and sintered magnets reported last year. This is a 40 percent gain in the residual induction. Because of low coercivities in the present samples, the energy products are quite low. However, the coercivities should increase by a slight increase in the ratio of rare earth to cobalt ratio.



TSA 2126

Figure 11. Microstructure of sample #H-4 in as-HIP'ed condition. 200x



TSA 2127

Figure 12. Microstructure of sample #H-15 in as-HIP'ed condition. 200x

The measured  $(BH)_{\max}$  values are shown in the table along with the potential  $(BH)_{\max}$  values in the next column which would be the case if we produce higher coercivities. The improvement in the  $B_r$  values in the case of the Tb-Sm-Co composition is not as pronounced as in the case of the Er-Sm-Co magnets. However, only one sample (H-4) of the HIPed Tb-Sm-Co magnet had similar composition as the die-pressed and sintered magnets. The gain in  $B_r$  achieved in this magnet is about 16 percent.

Only four of the HIPed samples had high enough coercivity to permit measurement of the temperature coefficient by the apparatus we had developed for such measurements. The results shown in the last column of Table 3 show that the temperature coefficients of these magnets are between +30 and -30 ppm/°F for Tb-Sm-Co magnets and -20 ppm/°F for only Er-Sm-Co magnet. The zero temperature coefficients in both Er-Sm-Co and Tb-Sm-Co appear to be somewhere about 35 wt %  $\text{HfCo}_5$  + 65 wt %  $\text{SmCo}_5$  agreeing generally well with findings reported last year using sintered magnets.

X-ray diffractometer traces were taken on the following samples: (1) Er-Co and Tb-Co alloy powders, (2) surface and powder patterns of samples H-2 and H-11 following the heat treatment of Table 3. The results of the x-ray diffraction analysis are as follows:

Both the alloys Er-Co and Tb-Co produced the same patterns as  $\text{SmCo}_5$ . The peak positions were slightly shifted from those of the  $\text{SmCo}_5$  peaks. The powder patterns of samples H-2 and H-11 were again very similar to  $\text{SmCo}_5$  powder pattern with the peak position intermediate between  $\text{TbCo}_5$  and  $\text{SmCo}_5$  for H-2 and intermediate between  $\text{ErCo}_5$  and  $\text{SmCo}_5$  for H-11. For each h,k,l plane, there was only a single sharp line, indicating homogeneous solid solution between the 1-5 compounds. The surface patterns taken off the planes perpendicular to the magnetization direction showed strong 00.2 khl line, indicating good magnetic alignment.

From the studies carried out thus far on the two ternary systems, Er-Sm-Co and Tb-Sm-Co, the following observations are drawn.

- (1) Near-zero temperature coefficients of  $B_r$  can be obtained in  $\text{ErCo}_5 + \text{SmCo}_5$  and  $\text{TbCo}_5 + \text{SmCo}_5$  at compositions of 35 to 40 weight percent  $\text{ErCo}_5$  and 30-35 weight percent  $\text{TbCo}_5$ , respectively for the temperature range of 140° to 160°F.
- (2) The maximum energy products, with good alignment and high coercivity in the zero coefficient magnets would be 13 to 15 MGOe for Er-Sm-Co and 7 to 9 MGOe for Tb-Sm-Co.

## SECTION 3

### Sm-Co MAGNETS BY PLASMA SPRAYING

#### 3.1 Objective

The objective of this task is to investigate the feasibility of employing arc-plasma-spraying as a process for producing  $\text{Sm}_2\text{Co}_{17}$  type magnets of binary Sm-Co compositions with coercivities considerably higher than the 1 to 2 kOe that are obtained through the conventional sintering process. Examination of plasma spraying for  $\text{Sm}_2\text{Co}_{17}$  magnet fabrication was mainly motivated by our earlier successes with the  $\text{SmCo}_5$  composition.

#### 3.2 Background

Sintering is the most widely used technology for producing  $\text{SmCo}_5$  and  $\text{Sm}_2\text{Co}_{17}$  type magnets. The sequence of operation includes generation of fine alloy powder, alignment and compaction of this powder in an applied magnetic field, and sintering of the compact to achieve high density. This technique is presently capable of producing  $\text{SmCo}_5$  magnets with  $(\text{BH})_{\text{max}}$  of 16 to 20 mGOe<sup>(9)</sup> and  $\text{Sm}_2(\text{TM})_{17}$  magnets with energy products in excess of 30 mGOe (TM = Transition Metal).<sup>(10)</sup> In each of these instances, however, the value of  $H_{\text{Ci}}$  measured is considerably lower than what appears to be theoretically possible with these materials. The maximum  $H_{\text{Ci}}$  attainable is indicated by the value of the measured anisotropy field,  $H_A$ , in these materials. These values are about 350 kOe for  $\text{SmCo}_5$  and close to 100 kOe for  $\text{Sm}_2\text{Co}_{17}$ .<sup>(11)</sup> The actual values obtained in these materials for sintered magnets are in the range of 15 to 35 kOe for  $\text{SmCo}_5$ , about 1 to 2 kOe for  $\text{Sm}_2\text{Co}_{17}$ , and roughly 15 kOe for the modified  $\text{Sm}_2(\text{TM})_{17}$  compositions. These low  $H_{\text{Ci}}$  values have been attributed by various researchers to effects arising from oxidation, microcracking and grain growth.<sup>(12)</sup> While these low  $H_{\text{Ci}}$

values may be suited for some general applications, they are particularly discouraging for applications that demand constant flux over extended periods of time.

All of the effects discussed above are known to play a strong role in determining  $H_{ci}$  in  $SmCo_5$  magnets. In the case of the  $Sm_2Co_{17}$  type compositions, however, these aspects take on added significance (in the fabrication of this latter material). Experimental efforts to produce reasonably high  $H_{ci}$   $Sm_2Co_{17}$  magnets have so far been very disappointing.

### 3.3 Rationale for Adopted Approach

The single most important parameter for successful inertial applications is magnet flux stability at gyro operating temperatures. Experiments at CSDL have shown that sprayed  $SmCo_5$  magnets show a remarkably lower rate of flux decay than do commercial magnets.<sup>(13)</sup> This is primarily the result of the very high quality of material that has been produced with this process. Sprayed  $SmCo_5$  magnets, however, are close to isotropic and, therefore, the energy product of these magnets is close to half of what is obtained in the aligned, commercially fabricated material. To obtain a higher amount of flux from these magnets, one needs to either introduce texture in the deposits or to shift the material composition towards higher cobalt content (by spraying  $Sm_2Co_{17}$  type of deposits).

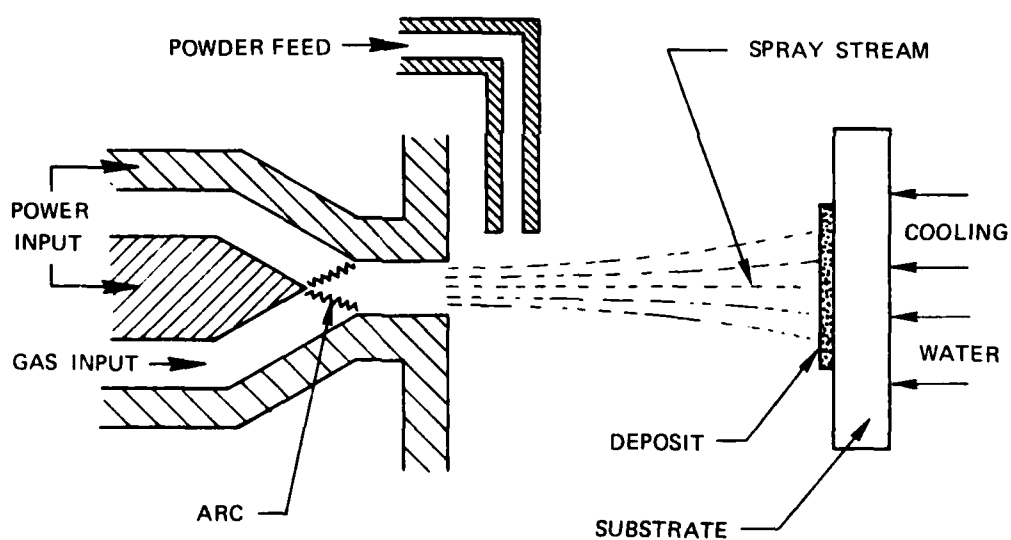
An isotropic  $Sm_2Co_{17}$  magnet is expected to show an energy product of about 10 to 12 MGOe as opposed to 7 to 9 MGOe measured in isotropic  $SmCo_5$  material and 16 to 18 MGOe found for aligned commercial  $SmCo_5$  magnets. An aligned  $Sm_2Co_{17}$  magnet would obviously show much higher values.



To date, efforts employing sintering of aligned  $\text{Sm}_2\text{Co}_{17}$  magnets have been unsuccessful in fabricating magnets with acceptable levels of the intrinsic coercivity ( $H_{ci}$ ). The maximum value of  $H_{ci}$  measured on binary  $\text{Sm}_2\text{Co}_{17}$  sintered material is about 1 to 2 kOe as opposed to a theoretical maximum possibility of about 100 kOe. In contrast, CSDL's sprayed  $\text{SmCo}_5$  magnets have exhibited coercivities of 68 kOe.<sup>(12)</sup> This research deals with the production of higher values of intrinsic coercivity using the plasma spray process for isotropic  $\text{Sm}_2\text{Co}_{17}$  deposits with potential energy products on the order of 12 MGOe.

### 3.4 The Plasma Spray Process

A schematic sketch of this process is shown in Figure 13.



10/77 12404 REV A 1/78

Figure 13. Schematic sketch of spray process.<sup>(14)</sup>

The process involves striking a high intensity dc arc between two electrodes, and ionization of gases - nitrogen, hydrogen, argon, and helium - as a consequence. This forms the plasma. Upon exit through a nozzle, the plasma combines to form neutral atoms, and releases a large amount of thermal energy without an appreciable loss in gas temperature. The material to be deposited is introduced at this stage in the form of a powder. The gases impart both thermal and kinetic energy to the powder particles, thereby melting them and propelling them rapidly towards the substrate to form the deposit.

### 3.5 Previous Work

Experience with spray fabrication of Sm-Co materials has shown that roughly 3 to 5 percent samarium is lost, relative to the cobalt (depending on the starting composition), through evaporation, during spraying. Also, an additional 1 percent is sacrificed to oxygen, both as a result of some oxygen present in the starting alloy and some that is picked up during processing. (The assumption that all of the oxygen in the deposit exists as an oxide of samarium appears reasonable in that  $\text{Sm}_2\text{O}_3$  has the lowest free energy of formation amongst the several possible oxides that can be considered.) Based on these considerations, five compositions were selected in the range of 26.0 to 34.0 weight percent samarium and sprayed on water-cooled copper substrates inside an inert gas environment plasma spray chamber. The deposits were kept reasonably thin (about 0.3 cm) on purpose, since a greater level of crystallinity is known to develop in plasma-sprayed deposits with increasing deposit thickness during spraying.<sup>(14)</sup> The as-sprayed microstructures appeared with a pancake-type morphology resulting from flattening of the molten alloy particles upon impact at the substrate.<sup>(12)</sup> The as-sprayed structures also contained pores (which appeared as dark, almost circular regions) and a few unmelted particles, in addition to the observed platelets which give rise to the layered microstructure.

X-ray diffraction patterns were obtained on a few of the deposits with copper radiation and a diffracted beam graphite monochromator.

Considerable broadening of the X-ray peaks was observed for all of the deposits. The diffuse patterns obtained on these materials were believed to be indicative of amorphous structures similar to what are conventionally obtained by rapid quenching techniques. The existence of a few minor crystalline peaks was interpreted to indicate the existence of a small amount of crystalline material dispersed in an otherwise amorphous material. Along these lines a most interesting, and possibly very significant, observation was made for one of the deposited samples. The X-ray pattern obtained from the surface of this sample consisted of a single, sharp crystalline peak superposed on an otherwise amorphous type pattern. A single peak was interpreted as illustrative of texture in the crystalline component of the deposit. The composition of the deposit, as measured by the X-ray fluorescence technique, was indicated to be about 30.0 weight percent samarium (which is in the two-phase  $\text{SmCo}_5$  -  $\text{Sm}_2\text{Co}_{17}$  region of the phase diagram). The sole crystalline peak observed was found to be located at the (00.6) peak position for  $\text{Sm}_2\text{Co}_{17}$  - the compound of interest. This observation showed that if proper cooling conditions were maintained at the substrate it might be possible to produce crystallographically aligned  $\text{Sm}_2\text{Co}_{17}$  materials by plasma spraying, a feature that has so far eluded efforts on the  $\text{SmCo}_5$  sprayed materials.

A series of low temperature treatments were performed at varying time and temperature and the maximum value of coercivity measured using these procedures was 7.9 kOe. This deposit was produced from Sm-Co powder with a starting composition of 34 weight percent samarium. The other magnetic properties measured for this sample were  $B_R$  - 6500,  $H_C$  - 4050, and  $(BH)_{\text{max}} = 6.6$  MGOe. The substantial improvements observed for the magnetic properties with the low temperature treatments were attributed to increased homogenization and grain growth through crystallization-related processes. The dependence of an optimal thermal treatment procedure, on deposit composition was found to be at best minimal indicating that grain size played a strong role in determining the value of  $H_{C1}$  in these binary compositions. It was concluded that, if alignment of the  $\text{Sm}_2\text{Co}_{17}$  phase could be successfully controlled, magnets with superior energy products could conceivably result through the use of the lower temperature thermal treatments.

### 3.6 Present Work

#### 3.6.1 Deposit Fabrication

Several additional deposits were fabricated using starting powder compositions of roughly 42.0, 34.5, and 28.3 weight percent samarium. The X-ray diffraction patterns obtained using copper radiation with a diffracted beam graphite monochromator, in each of these cases, were observed to be representative of more crystalline material than was produced during the last reporting period. The peaks were still very broad, indicating that the grain size must still be extremely small. The diffraction patterns obtained on some of these deposits in the as-sprayed condition are shown in Figure 14. Additional experiments aimed at providing more cooling to the substrate through the use of liquid-nitrogen-chilled helium gas similarly did not appreciably alter this situation. The diffraction patterns obtained from these latter materials are shown in Figure 15. (These additional experiments were performed in an effort to be able to determine the correct conditions that would permit microstructure duplication of deposits that were produced earlier. These earlier deposits had shown evidence of what was interpreted as alignment of the  $\text{Sm}_2\text{Co}_{17}$  phase. So far these efforts have not met with much success.)

#### 3.6.2 Effect of Low Temperature Treatments in Hydrogen

Interesting observations were made when deposits produced from 42.0, 34.5, and 28.3 weight percent samarium powders were subjected for 16 hours to a low temperature (550°C) exposure to hydrogen at a pressure close to atmospheric. These experiments were performed to study the dependence of the effect of this hydrogen treatment on deposit composition. Earlier experiments with close-to-stoichiometric  $\text{SmCo}_5$  deposits had indicated that this results in the removal of internal stresses due to an increased atom mobility in a hydrogen atmosphere. (15)

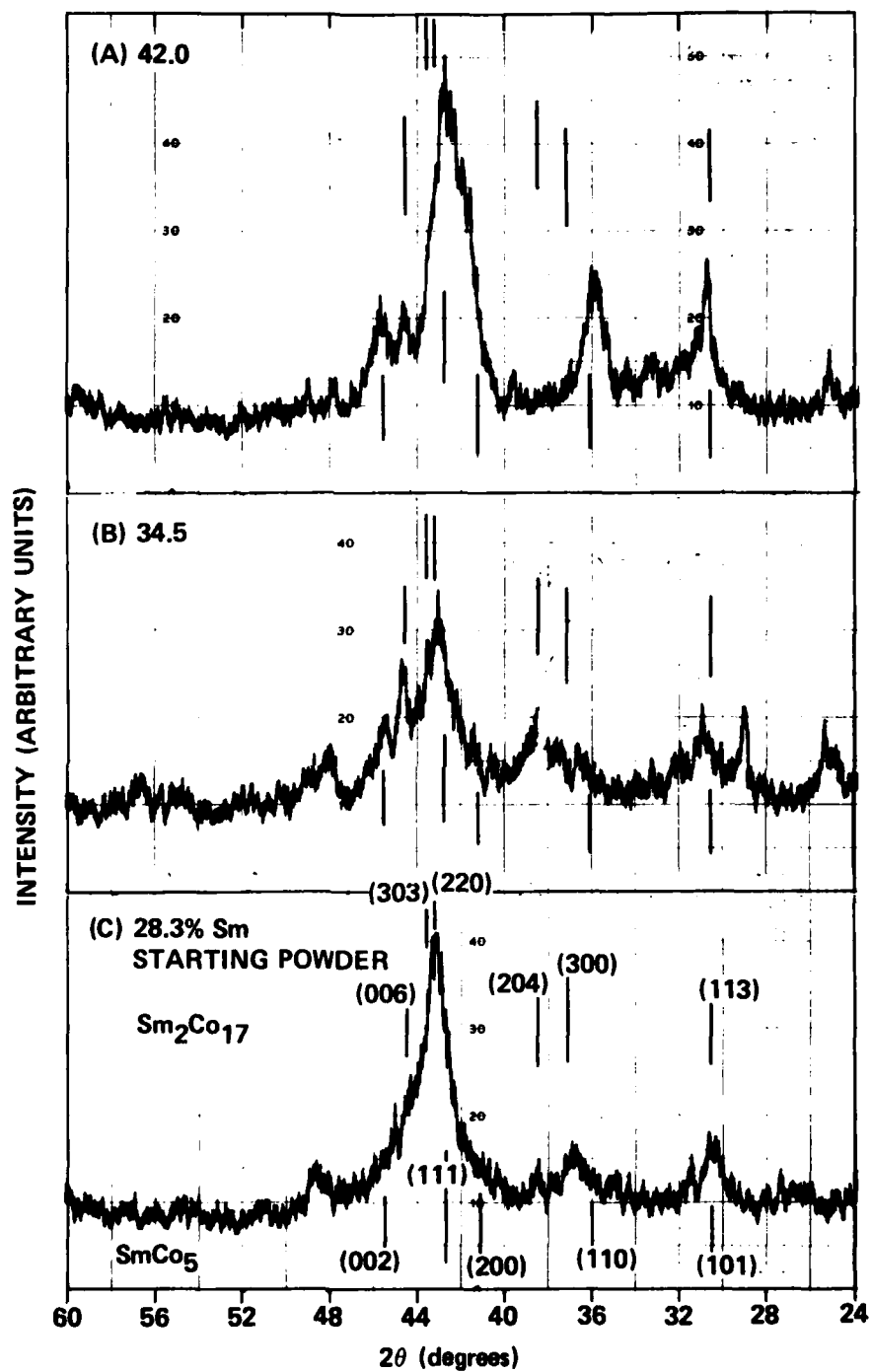


Figure 14. X-ray diffraction patterns on deposits formed from (A) 42.0, (B) 34.5, and (C) 28.3% Sm starting powder compositions.

2/81 CD22586



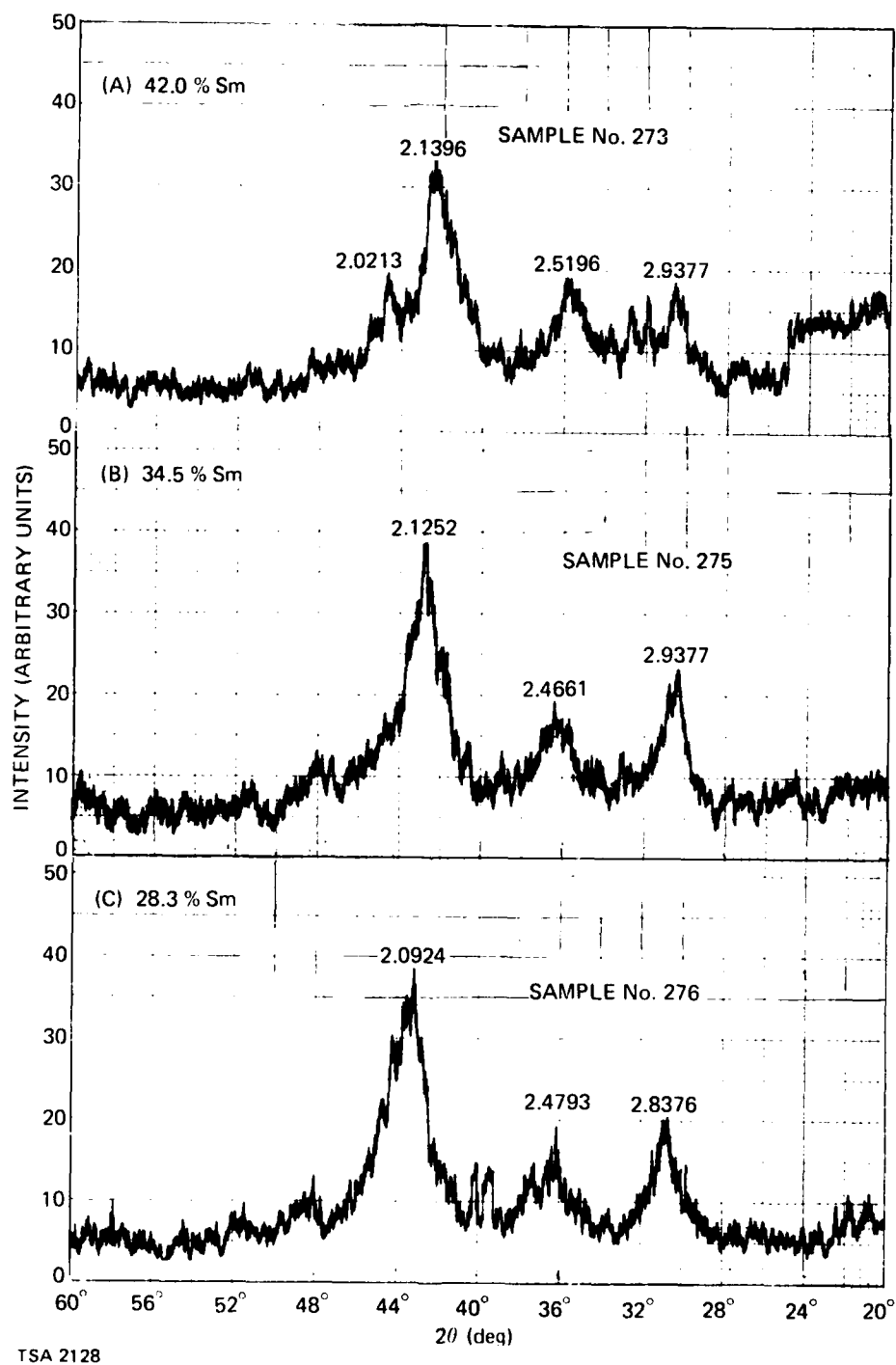


Figure 1. X-ray diffraction patterns on deposits formed on liquid nitrogen-chilled helium gas substrates. (A) 42.0, (B) 34.5, and (C) 28.3% Sm starting powder compositions.

It was therefore considered desirable to study if this effect persisted over a wide composition range. Use of such an atmosphere might be desirable during selected heat treatments of these compositions, performed with the aim of introducing texture into the material. As stated earlier, these deposits showed that they were composed of material which had a low level of crystallinity associated with it. (The diffraction peaks were still very broad, indicating an extremely small effective grain size.) Upon exposure to the hydrogen treatment described above, the surfaces of several samples were observed to yield almost identical, reasonably well defined sharp diffraction patterns. The X-ray diffraction patterns obtained on these samples following the hydrogen treatment are shown in Figure 16. (The as-sprayed structures of this series of specimens are indicated by the X-ray patterns of Figure 14 which were also made earlier on these very same specimens.) The original peaks were found to all but disappear from this hydrogen treatment.

When these deposits were given an additional 16-hour treatment under argon at 450°C and diffraction patterns were obtained, the well-defined (hydride) patterns were once again generated. All of the data that were obtained are shown in Table 4. This was somewhat contrary to expectations in that earlier observations had indicated that this type of treatment was capable of removing the effects related to hydrogen in the material.<sup>(15)</sup> All of the patterns obtained after the argon treatment are shown in Figure 17. To resolve this discrepancy, roughly 0.002 inch of material was removed from the surface of the 42 weight percent samarium starting powder deposit (exposed to both hydrogen and argon). When the freshly exposed surface was examined again using X-ray diffraction, a very low level of crystallinity was found to be retained. The hydride pattern was no longer observed and the weak lines on the diffraction pattern also were quite different than those observed in the as-sprayed condition. These observations were confirmed subsequently by obtaining long-term (16 hours) exposure Debye-Scherrer patterns. It was found that an eight-hour Debye-Scherrer exposure using  $\text{Cu}_{K\alpha}$  radiation resulted in only one line being detected at an interplanar spacing,  $d$ , of about 2.0 Å.

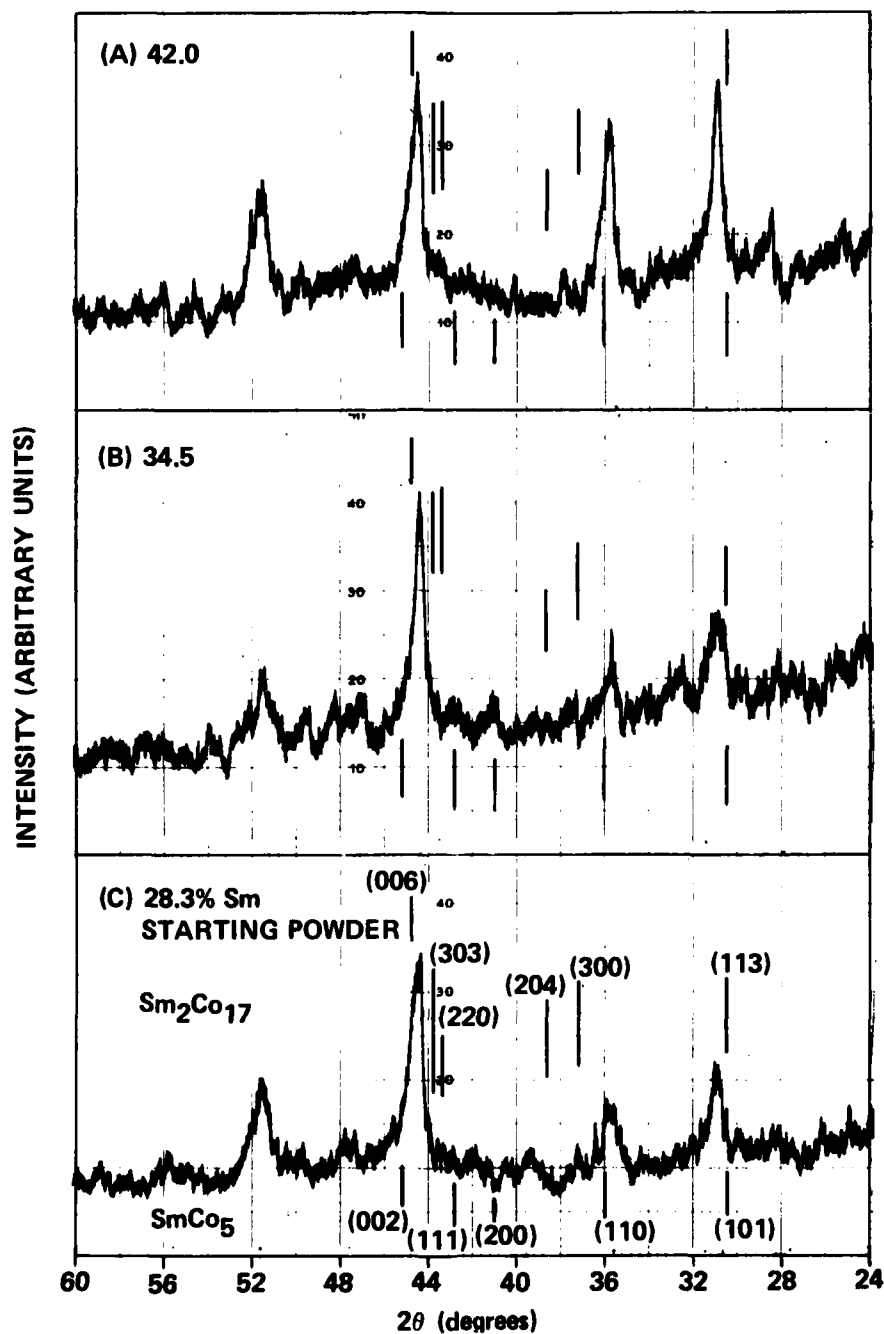


Figure 16. X-ray patterns obtained on samples in Figure 15 after 550°C, 16 hours exposure in hydrogen.

2/81 CD22588

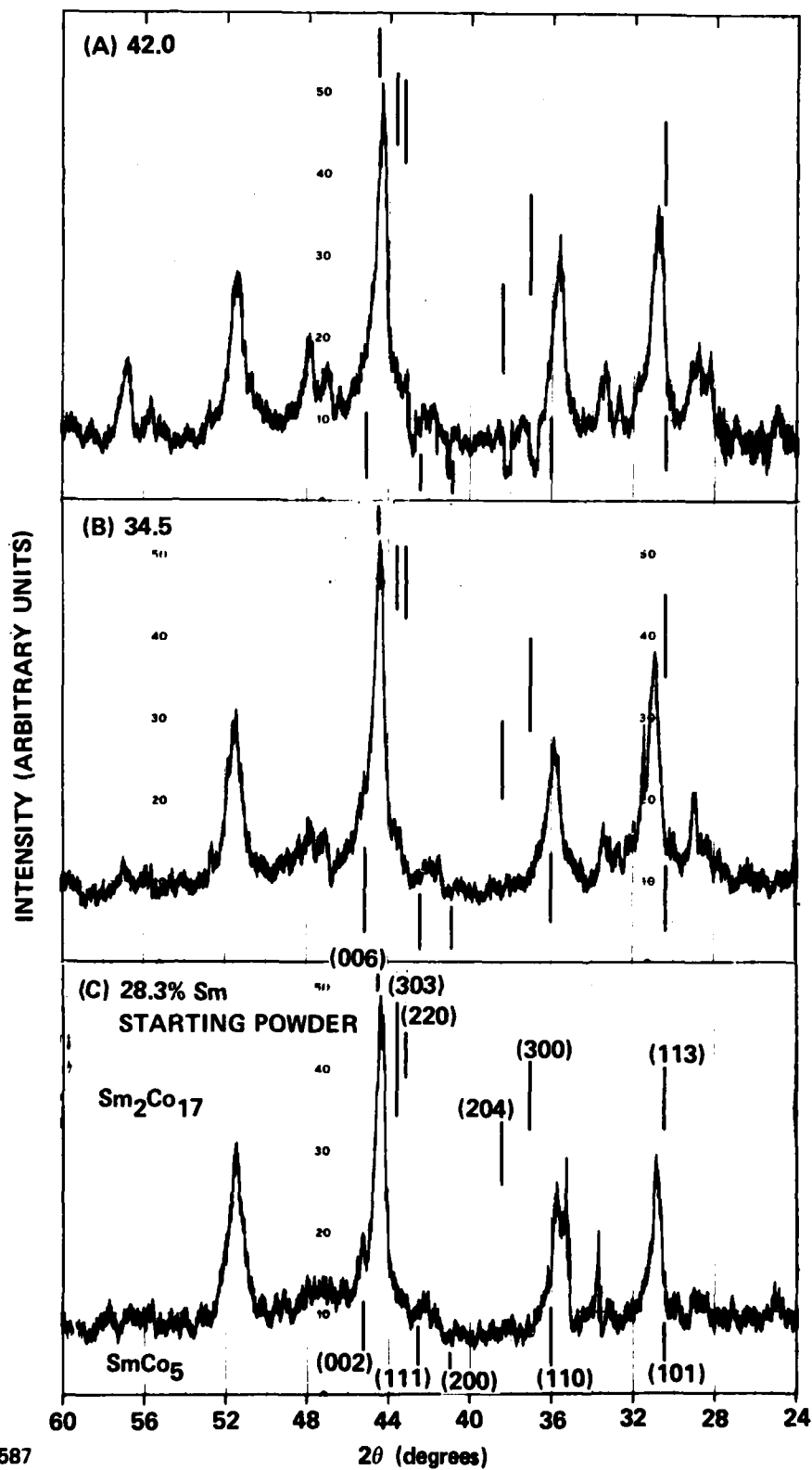




Table 4. X-ray data on 42.0, 34.5, and 28.3% Sm powder deposits after the several indicated heat treatments.  
(X-ray data on effects of H<sub>2</sub> and Argon with respect to Sample 266 are shown in Table 5.)

| Sample (Composition, Heat Treatment) |                  |                |                  |               |                  |                            |                  |                            |                  |                                     |                  |                                     |                  |
|--------------------------------------|------------------|----------------|------------------|---------------|------------------|----------------------------|------------------|----------------------------|------------------|-------------------------------------|------------------|-------------------------------------|------------------|
| 266(AS 42%)                          |                  | 267 (AS 34.5%) |                  | 268 (AS 28.3) |                  | 267(550°C,H <sub>2</sub> ) |                  | 268(550°C,H <sub>2</sub> ) |                  | 267(550°C,H <sub>2</sub> ,450°C Ar) |                  | 268(550°C,H <sub>2</sub> ,450°C Ar) |                  |
| d(Å)                                 | I/I <sub>0</sub> | d(Å)           | I/I <sub>0</sub> | d(Å)          | I/I <sub>0</sub> | d(Å)                       | I/I <sub>0</sub> | d(Å)                       | I/I <sub>0</sub> | d(Å)                                | I/I <sub>0</sub> | d(Å)                                | I/I <sub>0</sub> |
| 3.53                                 | W                | 3.52           | W                |               |                  |                            |                  |                            |                  |                                     |                  |                                     |                  |
|                                      |                  | 3.08           | W                |               |                  |                            |                  |                            |                  |                                     |                  |                                     |                  |
| 2.90                                 | S                | 2.88           | M                | 2.91          | S/M              | 2.88                       | S                | 2.89                       | S                | 2.88                                | S                | 2.88                                | S                |
| 2.49                                 | S                |                |                  |               |                  | 2.52                       | M                | 2.52                       | M                | 2.51                                | M                | 2.52                                | S                |
|                                      |                  | 2.35           | M                | 2.43          | M                |                            |                  |                            |                  |                                     |                  |                                     |                  |
|                                      |                  |                |                  | 2.34          | VW               |                            |                  |                            |                  |                                     |                  |                                     |                  |
| 2.16                                 | VVS              | 2.11           | VVS              | 2.09          | VVS              |                            |                  |                            |                  |                                     |                  |                                     |                  |
| 2.03                                 | M/W              | 2.03           | M                | 2.01          | W                | 2.04                       | VS               | 2.03                       | VS               | 2.03                                | VS               | 2.04                                | VS               |
| 1.98                                 | M                | 1.99           | M                |               |                  |                            |                  |                            |                  |                                     |                  |                                     |                  |
|                                      |                  | 1.89           | M/W              | 1.87          | W                | 1.77                       | M                | 1.77                       | S                | 1.77                                | M                | 1.77                                | S                |

AS = As-sprayed  
H<sub>2</sub> = Hydrogen exposure  
Ar = Argon exposure



2/81 CD22587

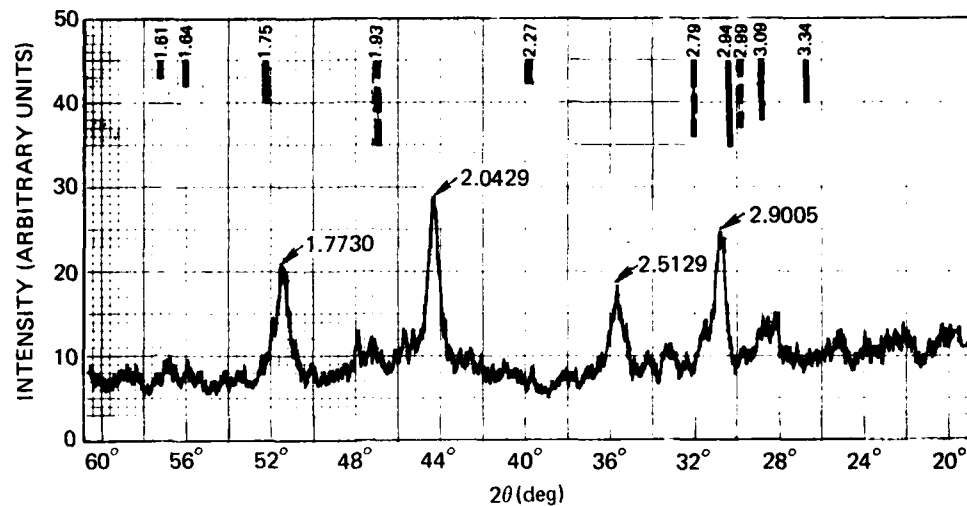
Figure 17. X-ray patterns obtained on samples in Figure 17 after an additional 450°C, 16 hours exposure in hydrogen.

When the exposure time was increased to 16 hours, two additional very weak lines were observed. Use of  $\text{Mo K}\alpha$  radiation and an exposure time of 16 hours, however, resulted in the appearance of a total of six lines. The 'd' spacings measured for the several peaks observed in this sample in the various conditions of heat treatment are listed in Table 5.

It was suspected that the removal of the low level of crystallinity by these treatments, initially observed in the bulk of the material, resulted from chemical interaction (absorption and desorption) of the hydrogen gas with the microcrystallites that were present. Because of the inhomogeneities that are known to be present in as-sprayed microstructures, compositions other than those for  $\text{SmCo}_5$  and  $\text{Sm}_2\text{Co}_7$  were retained because of no effect of the hydrogen atmosphere on their crystal structures. This observed removal of a low level of crystallinity, however, appeared to be in contradiction with some conclusions reached earlier from specific heat and magnetic property data.<sup>(15)</sup> The observations were nevertheless considered significant in that the nature of the interaction with hydrogen of the several "microcrystalline" deposits was found to be essentially similar over a broad range of deposit composition. The observation that the hydride phase existed in the surface regions even after the 450°C argon treatment (following the exposure to hydrogen) was also intriguing. This hydride compound was not specifically identified. Since the hydride phase was absent in the bulk, and the as-sprayed, low level of crystallinity was removed, these observations suggested that the (hydride) phase was somehow stabilized in the surface regions of the sample, possibly due to the presence of an oxide skin. A close examination of the X-ray patterns obtained, however, did not show peaks strongly characteristic of the oxide of samarium. (Because of the large negative free energy of formation of samarium oxide, compared to the oxides of cobalt, it was assumed that all oxygen would essentially exist as  $\text{Sm}_2\text{O}_3$ ). The 42.0 weight percent samarium pattern of Figure 16(A) is shown again as Figure 18 with the peak positions indicated for the compound(s)  $\text{Sm}_2\text{O}_3$ .

Table 5. X-ray data on 42.0% Sm powder deposit, obtained after the heat treatments indicated.

| Sample (Heat Treatment) |                  |                            |                  |                                   |                  |  |                  |   |                  |
|-------------------------|------------------|----------------------------|------------------|-----------------------------------|------------------|--|------------------|---|------------------|
| 266(AS)                 |                  | 266(550°C,H <sub>2</sub> ) |                  | 266(550°,H <sub>2</sub> ,450° Ar) |                  | 266 (550°C, H <sub>2</sub> , 450°C, Ar)<br>Surface Layer Removed |                  |   |                  |
|                         |                  |                            |                  |                                   |                  | Mo , 16 hr<br>K $\alpha$<br>(Crushed Powder)<br>Debye-Scherrer   |                  | Cu <sub>K<math>\alpha</math></sub> , 16 hr*<br>Debye-Scherrer |                  |
| d(Å)                    | I/I <sub>0</sub> | d(Å)                       | I/I <sub>0</sub> | d(Å)                              | I/I <sub>0</sub> | d(Å)   | I/I <sub>0</sub> | d(Å)  | I/I <sub>0</sub> |
| 3.53                    | W                |                            |                  |                                   |                  |  |                  | 3.07  | W                |
| 2.90                    | S                | 2.88                       | VS               | 2.88                              | S                | 3.08   | S                | 2.7   | VW               |
| 2.49                    | S                | 2.50                       | S                | 2.50                              | S                |  |                  |   |                  |
| 2.16                    | VVS              |                            |                  |                                   |                  |  |                  |   |                  |
| 2.03                    | M/W              | 2.03                       | VS               | 2.03                              | VS               | 2.07   | S/M              | 2.0   | S                |
| 1.98                    | M                | 1.77                       | S/M              | 1.77                              | S/M              | 1.89   | M                |   |                  |
|                         |                  |                            |                  |                                   |                  | 1.61   |                  |   |                  |
|                         |                  |                            |                  |                                   |                  | 1.25   |                  |   |                  |



SOLID VERTICAL LINES DENOTE 3 STRONGEST PEAKS FOR  $\text{Sm}_2\text{O}_3$  (FILE NO. 19-1114)

DASHED VERTICAL LINES DENOTE 3 STRONGEST PEAKS FOR  $\text{Sm}_2\text{O}_3$  (FILE NO. 11-412)

TSA 2129

Figure 18. Sample in Figure 17(A) showing expected "d" spacings for the compound  $\text{Sm}_2\text{O}_3$ .

### 3.6.3 Experiments on Annealing in a Magnetic Field

There are a number of possible avenues one could pursue to crystallize the sprayed non-crystalline material in such a way as to give it a desired crystallographic texture. The desired texture of course is one where the c-axis of all individual grains (crystallites) is parallel. Both  $\text{SmCo}_5$  and  $\text{Sm}_2\text{Co}_{17}$  have hexagonal close-packed symmetry, with the c-axis in both cases being the easy magnetization direction. With the anisotropic structure as above the material should have the highest possible residual induction when magnetized in the c-axis direction.

The present effort deals with the crystallization of plasma sprayed Sm-Co alloy deposits in an applied high strength magnetic field. The crystallization temperature of amorphous  $\text{SmCo}_5$  is approximately 500°C. Therefore, if an amorphous plasma spray deposit is heated from room temperature to an elevated temperature past the 500°C in a strong dc magnetic field, the crystal nuclei formed, might have their c-axis parallel to the applied field. As these nuclei grow by incorporating the surrounding amorphous alloy into their crystal lattices a preferred orientation in the mass can result with the c-axis of the various grains oriented parallel to each other (the direction of the applied magnetic field) and random orientation of the basal planes perpendicular to the c-axis.

A six-inch bore Bitter magnet capable of producing a dc magnetic field of about 80 kOe was made available by the National Magnet Laboratory of MIT for this study. An available furnace capable of operating inside the Bitter magnet was modified for carrying out magnetic annealing experiments. A schematic drawing of the longitudinal section of the furnace is shown in Figure 19. The cylindrical furnace fitted snugly in the bore of the 6-inch magnet. The sample was located inside a stainless steel tube at the peak position of the magnetic field and was heated by 4 SiC rods. Temperature control and rate of rise of temperature were controlled manually using a Variac power supply. The temperature of the sample was determined by a thermocouple located inside the furnace tube adjacent to the magnet sample. The outer shell of the furnace was water-cooled to prevent undue heating of the Bitter magnet.

Plasma spray deposits of powders of following Sm-Co alloy compositions were used in the initial studies of magnetic annealing: (1) 42.0 wt % Sm, (2) 34.5 wt % Sm, (3) 28.3 wt % Sm. The stoichiometric intermetallic compounds  $\text{SmCo}_5$  and  $\text{Sm}_2\text{Co}_{17}$  contain 33.9 wt % and 23.1 wt % Sm respectively. Because of evaporation losses during plasma spraying normally the compositions Nos. (1) and (3) would produce deposits of close to stoichiometric  $\text{SmCo}_5$  and  $\text{Sm}_2\text{Co}_{17}$  respectively,

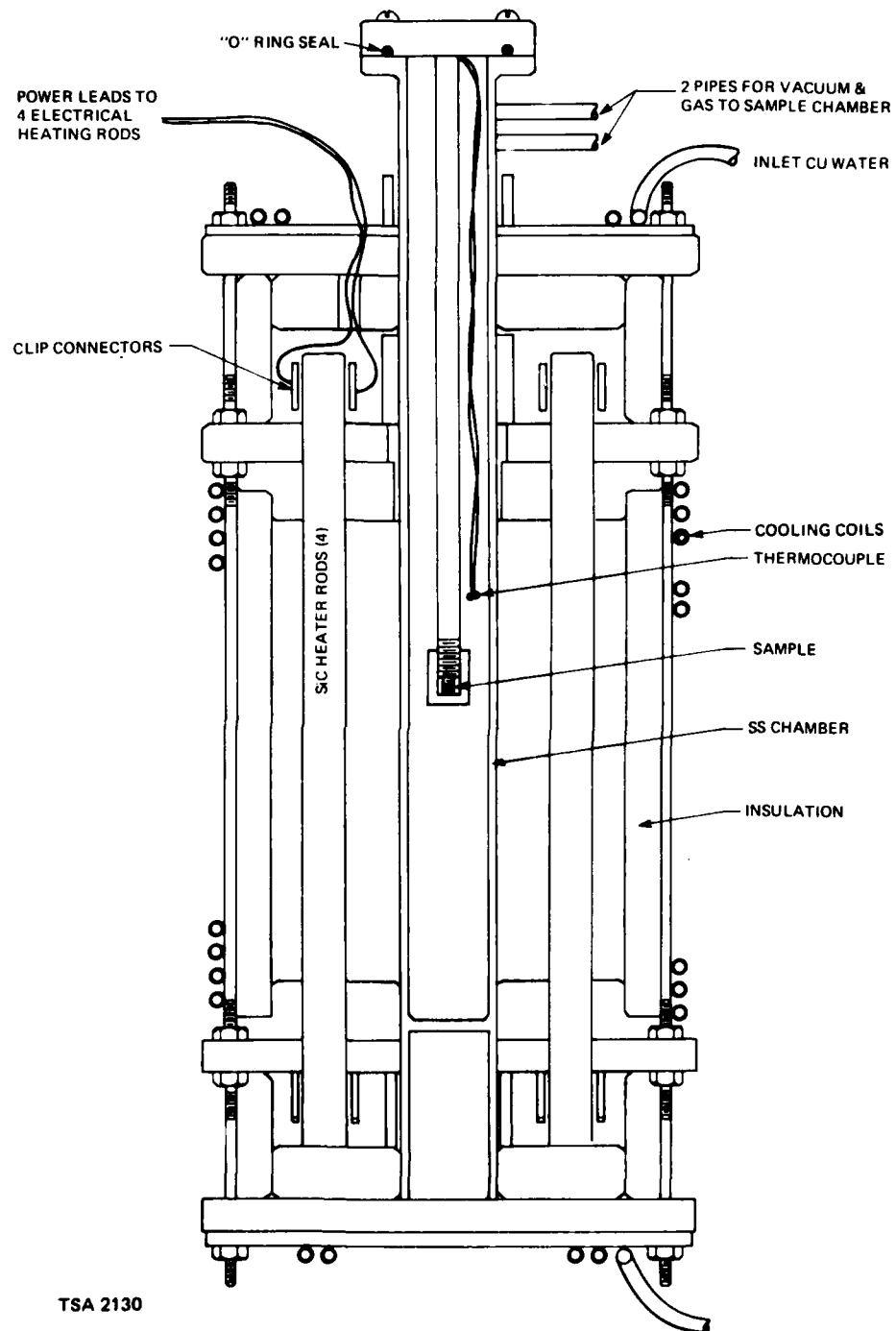


Figure 19. Schematic sketch of modified furnace used for magnetic annealing experiments.

and the intermediate composition (34.5 weight percent samarium) powder should produce a deposit which would be in the two-phase ( $\text{SmCo}_5 + \text{Sm}_2\text{Co}_{17}$ ) region. The selection of the above compositions therefore gave a comprehensive range for the study.

Two sets of samples were allowed to crystallize while subjected to the 80 kOe magnetic field. One set was given a heat treatment in a hydrogen atmosphere at 500°C for 16 hours prior to the magnetic annealing, and the other set was magnetically annealed in the as-sprayed condition. Each set was given a number of different thermal treatments. Following each thermal treatment, including the magnetic annealing, the magnetic properties of each sample were measured. The magnetic data corresponding to each thermal history are given in Tables 6 and 7 for the two sets with and without the hydrogen treatment.

Two important facts should be noted here. Although the crystallization temperature of these amorphous materials is around 500°C, it was determined earlier that the presence of a hydrogen atmosphere raises the crystallization temperature to about 700°C and enhances the mobility of the atoms.<sup>(15)</sup> Therefore, there was no danger of prior nucleation of the amorphous material during the 500°C hydrogen treatment; however, there was a chance of increasing the alignment in the subsequent magnetic annealing because of increased atom mobility. The other fact is that in all cases of magnetic annealing the sample was heated to 400°C before the magnetic field was applied, since little, if any, nucleation was expected to occur up to that temperature. More important, this procedure saved about 500 kilowatt-hours of electrical power.

In addition to the two sets of samples that were magnetically annealed, a 42.0 weight percent samarium sample was given similar heat treatments as the two batches but without the magnetic anneal. The data that was obtained are shown in Table 8. The  $4\pi M$  versus  $H$  curves obtained on the 42.0 weight percent samarium samples after the various treatments are shown in Figures 20 through 22.



Table 6. Magnetic properties of thermally-treated magnetically annealed Sm-Co deposits without H<sub>2</sub> treatment.

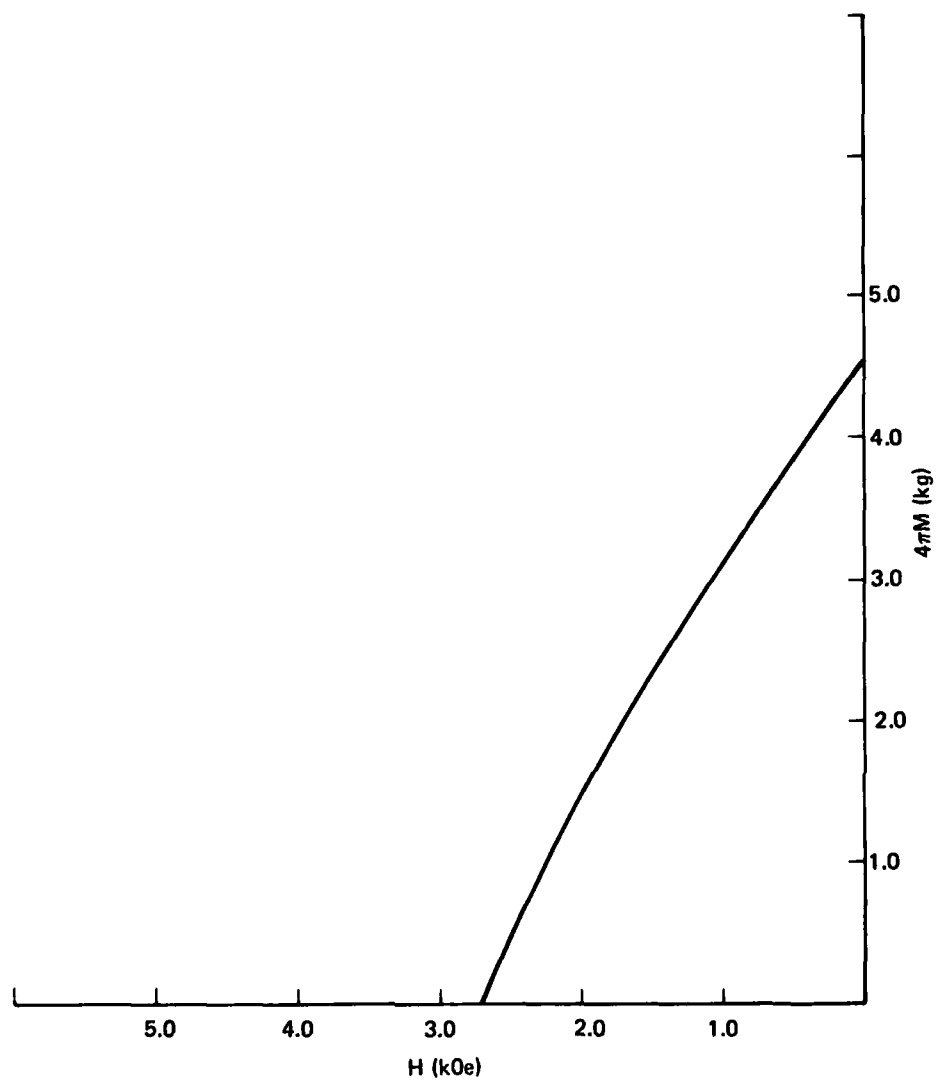
| Serial No. | Heat Treat Condition                       | % Sm in Spray powder | B <sub>R</sub> (G) | H <sub>C</sub> (Oe) | H <sub>C</sub> (kOe) | (BH) <sub>max</sub> (MGOe) |
|------------|--|----------------------|--------------------|---------------------|----------------------|----------------------------|
| (A)        | As Sprayed                                 | 42.0                 | 4450               | 3900                | 26.0                 | 4.3                        |
|            |  | 34.5                 | 5450               | 1650                | 2.5                  | 2.3                        |
|            |  | 28.3                 | 4650               | 300                 | 0.5                  | 0.3                        |
| (B)        | (A) + Magnetic Anneal 720°C<br>1 hour      | 42.0                 | 4700               | 4500                | 51.0                 | 5.3                        |
|            |  | 34.5                 | 5500               | 3450                | 6.5                  | 4.7                        |
|            |  | 28.3                 | 5300               | 2200                | 2.5                  | 2.9                        |
| (C)        | (B) + 1000°C-2 hrs<br>900°C-20 hrs<br>F.C. | 42.0                 | 5200               | 5050                | 59.0                 | 6.5                        |
|            |  | 34.5                 | 5100               | 2500                | 4.5                  | 3.2                        |
|            |  | 28.3                 | 4250               | 500                 | 1.0                  | 0.5                        |
| (D)        | (C) + 1100°C-2 hrs<br>900°C-20 hrs<br>F.C. | 42.0                 | 5850               | 5600                | 55.0                 | 8.2                        |
|            |  | 34.5                 | 51.50              | 2000                | 3.5                  | 2.8                        |
|            |  | 28.3                 | 4300               | 0                   | 0                    | 0                          |
| (E)        | (D) + 1135°C-2 hrs<br>900°C-20 hrs<br>F.C. | 42.0                 | 6200               | 6050                | 58.5                 | 9.4                        |
|            |  | 34.5                 | 4450               | 2000                | 8.0                  | 2.2                        |
|            |  | 28.3                 | 3100               | 0                   | 0                    | 0                          |

Table 7. Magnetic properties of thermally treated deposits magnetically annealed after H<sub>2</sub> treatment.

| Serial No. | Heat Treat Condition                         | % Sm of Powder | B <sub>R</sub> (G) | H <sub>C</sub> (Oe) | H <sub>ci</sub> (kOe) | (BH) <sub>max</sub> (MGoe) |
|------------|--|----------------|--------------------|---------------------|-----------------------|----------------------------|
| (A)        | As-Sprayed                                   | 42.0           | 4450               | 3900                | 26.0                  | 4.3                        |
|            |  | 34.5           | 5450               | 1650                | 2.5                   | 2.3                        |
|            |  | 28.3           | 4650               | 300                 | 0.5                   | 0.3                        |
| (B)        | (A) + 500°C, 16 hrs in H <sub>2</sub> , F.C. | 42.0           | 4700               | 2550                | 5.5                   | 3.0                        |
|            |  | 34.5           | 6100               | 0                   | 0                     | 0                          |
|            |  | 28.3           | 7000               | 0                   | 0                     | 0                          |
| (C)        | (B) + Magn. Anneal 1 hr at 720°C F.C.        | 42.0           | 4700               | 4500                | 55                    | 5.3                        |
|            |  | 34.5           | 5400               | 3100                | 5                     | 4.2                        |
|            |  | 28.3           | 5500               | 2200                | 2                     | 3.1                        |
| (D)        | (C) + 1140°C, 2 hr, 900°C, 24 hr, QC         | 42.0           | 6100               | 5900                | 58                    | 9.0                        |
|            |  | 34.5           | 5200               | 2500                | 4                     | 3.2                        |
|            |  | 28.3           | 3950               | 850                 | 1                     | 0.8                        |

Table 8. Magnetic properties of 42.0% Sm deposit without magnetic alignment.

| Serial No. | Heat Treat Condition  | $B_R$ (G) | $H_C$ (Oe) | $H_{ci}$ (kOe) | $(BH)_{max}$ (MGoe) |
|------------|---|-----------|------------|----------------|---------------------|
| (A)        | As-Sprayed  | 4450      | 3900       | 26.0           | 4.3                 |
| (B)        | (A) + No magnetic anneal<br>slow rise to 725°C,<br>1 hr, F.C. | 4600      | 4250       | 12.0           | 4.9                 |
| (C)        | (B) + Slow rise to 725°C,<br>24 hr, F.C.                      | 4450      | 4000       | 12.5           | 4.5                 |
| (D)        | (C) + 1140°C, 2 hrs<br>900°C, 20 hrs, QC                      | 5700      | 5600       | 63.0           | 7.9                 |



TSA 2131

Figure 20.  $4\pi M$  versus  $H$  behavior of as-sprayed deposit from 42.0% Sm powder.

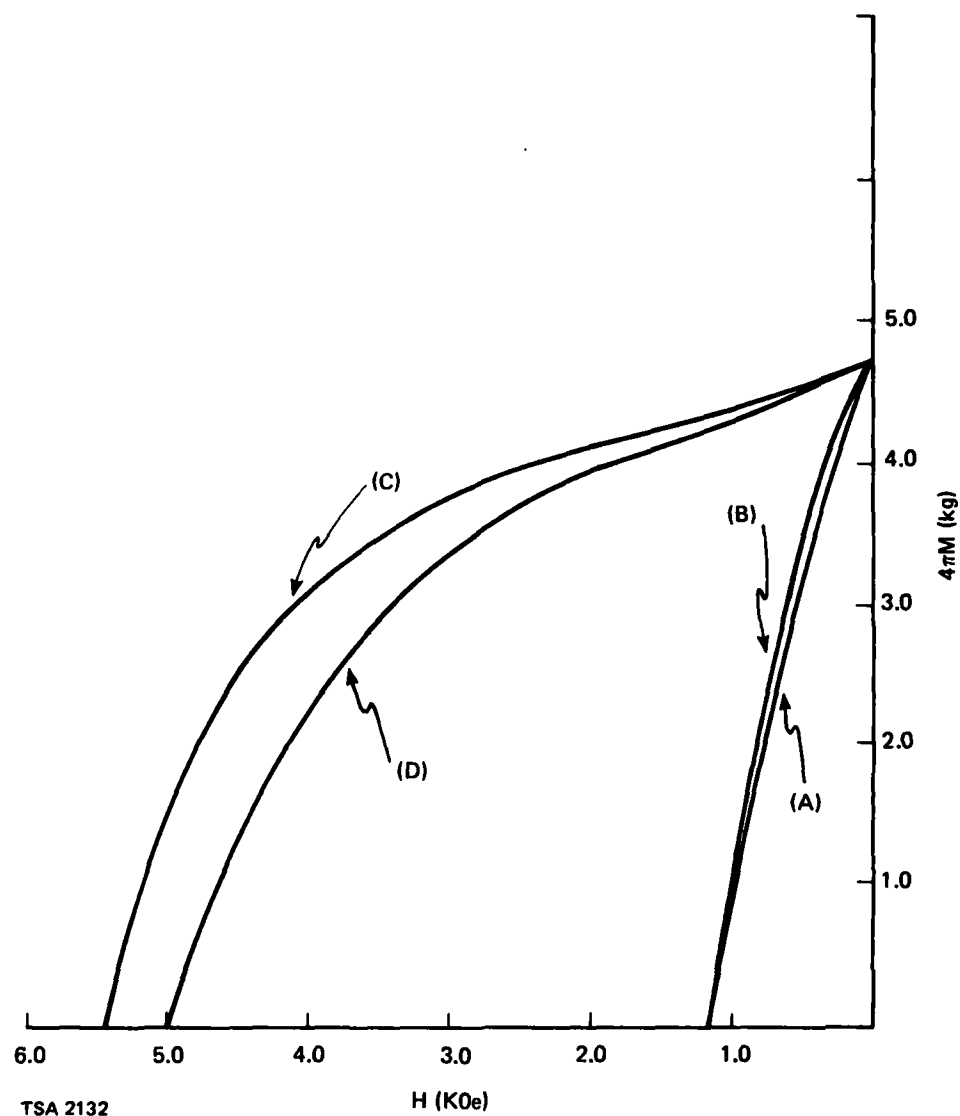


Figure 21.  $4\pi M$  versus  $H$  curves after (A):  $725^\circ\text{C}$ , 1 h, without applied field; (B): (A) +  $720^\circ\text{C}$ , 24 h without applied field; (C) and (D): Approx. 1.5 h duration rise from  $400^\circ\text{C}$  to  $720^\circ\text{C}$  under 80 kOe applied magnetic field. (C) corresponds to sample treated with  $\text{H}_2$  prior to magnetic anneal. (D) corresponds to sample without the  $\text{H}_2$  treatment.

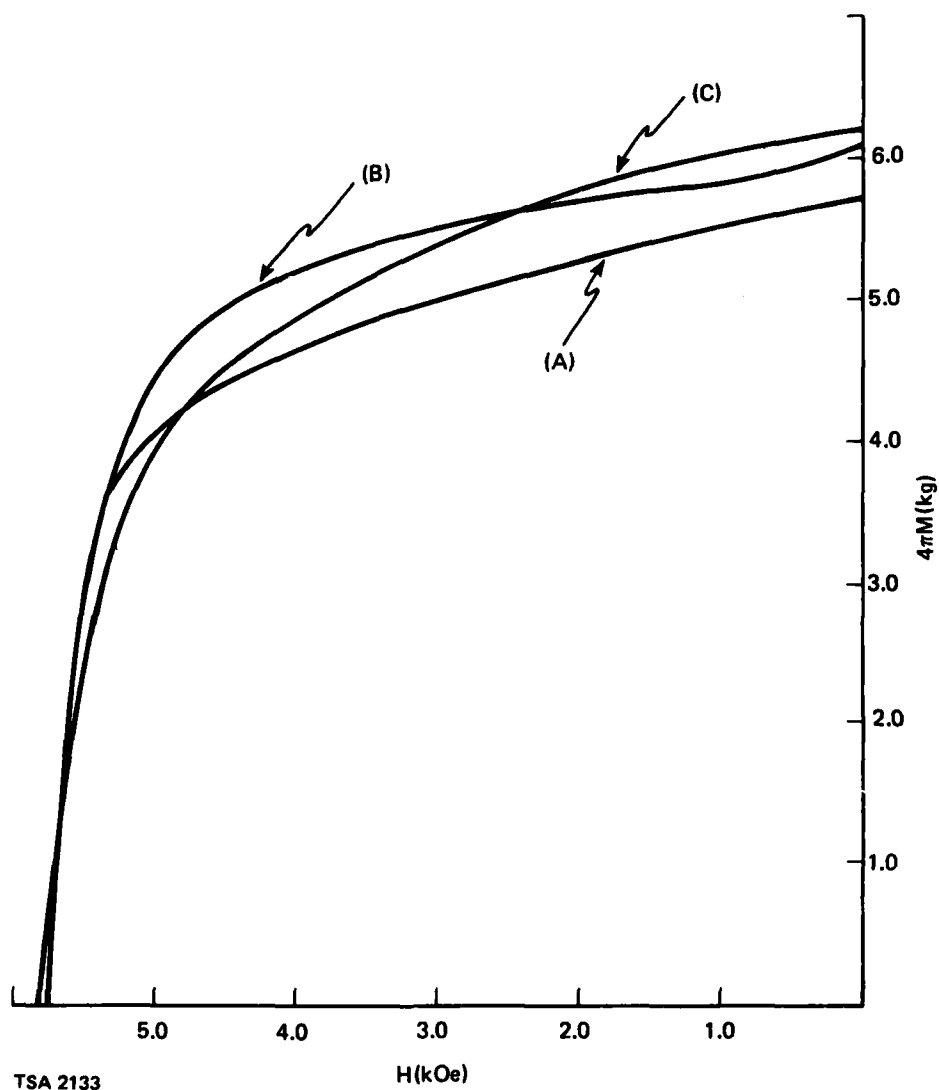


Figure 22. Demagnetization behavior after exposure: 1140°C, 2 hours + 900°C, 20 hours + quick cooling.

- (A) No magnetic annealing.
- (B) Magnetic annealing after  $H_2$  treatment.
- (C) Magnetic annealing without  $H_2$  treatment.

It is premature to draw firm conclusions about the magnetic alignment on the basis of these preliminary experiments. When we compare the samples after their treatment at the highest temperatures of about 1140°C, the magnetically aligned samples show 10 percent higher  $B_r$  and a consequent increase in the maximum energy product. This comparison is only true for deposits formed with a starting powder composition of 42.0 weight percent samarium (which resulted in a post-spray composition close to that of stoichiometric  $\text{SmCo}_5$ ). No comparisons could be made for the other two compositions containing the phase  $\text{Sm}_2\text{Co}_{17}$ , since data were not collected on samples of these compositions without the magnetic anneal. The magnetic properties of these other compositions were quite modest, even after the magnetic annealing; therefore, there appeared little need of examining these materials. The  $B_r$  values of over 6000 G in the 42.0 weight percent case indicated that there was a degree of alignment which was higher than random orientation. (The theoretically best value of  $B_r$  in the random case is about 5500 G for a fully dense material.) It is possible that one hour at 720°C temperature with the magnetic field may not have been sufficient to fully crystallize the material in the desired orientation. Higher temperature in the absence of valuable larger residence time in the high magnetic field may provide substantially more alignment than the present case.

Whereas the higher temperature treatments (without field) proved to be beneficial for the 42.0 weight percent samarium sample after the magnetic anneal, the other two compositions showed deterioration. A surprising observation was the large increase in coercivity observed for the 42.0 weight percent sample with the 720°C magnetic anneal. No such comparable coercivity increase was found for the sample where no magnetic field was applied. It is possible, however, that the actual temperature of the sample in the two cases of magnetic annealing was higher than that suggested by the thermocouple reading. If indeed the observations are valid, they suggest the positive effect of applying a magnetic field in that it appears to facilitate the homogenization process (which must account for the increased coercivity). More experiments are planned to confirm these preliminary observations.

#### REFERENCES

1. Das, D., E. Wettstein, and K. Kumar, Technical Report R-1177, Charles Stark Draper Laboratory, July 1978. Office of Naval Research Contract N00014-77-C-0388.
2. Das, D., K. Kumar, and E. Wettstein, Technical Report R-1306, Charles Stark Draper Laboratory, October 1979. Office of Naval Research Contract N00014-77-C-0388.
3. Das, D., K. Kumar, and E. Wettstein, Technical Report R-1435, Charles Stark Draper Laboratory, December 1980. Office of Naval Research Contract N00014-77-C-0388.
4. Benz, M.G., R.P. Laforce, and D.L. Martin, AIP Conf. Proc. No. 18, 1974, p. 1173.
5. Mildrum, H.F., and D.J. Iden, Goldschmidt Informiert, 4/75, No. 35, December 1975, p. 54.
6. Paladino, A.E., et al, IEEE Trans. Mag., Mag-11 (1975), p. 1455.
7. Jandeska, W.F., Proc 3rd Intnat'l Workshop on RE-Co Perm. Magnets, June 27-30, 1978, p. 450.
8. Das, D., and K. Kumar, IEEE Trans. on Magnetism, Vol. Mag-16, No. 5, (1980), p. 1000.
9. Das, D., IEEE Trans. Magn., MAG 5 (3), 1969, p. 214.
10. Yoneyama, T., A. Fukono, and T. Ojima, Summaries of the 3d Intl. Conference on Ferrites, Paper 30AB2-5, p. 97, Kyoto, Japan, 29 September - 2 October 1980.
11. Strnat, K.J., and A.E. Ray, Goldschmidt informiert, 4/75, p. 47.



#### REFERENCES (Cont.)

12. Kumar, K., D. Das, and E. Wettstein, J. Appl. Phys., 49 (3), 1978, p. 2052.
13. Kumar, K., D. Das, and C.R. Dauwalter (unpublished).
14. Kumar, K., and D. Das, Thin Solid Films, 54 (3), 1978, p. 263.
15. Kumar, K., D. Das, and R. Williams, J. Appl Phys., 51 (2), 1980, p. 1031.

# BASIC DISTRIBUTION LIST

| <u>Organization</u>   | <u>Copies</u> | <u>Organization</u>  | <u>Copies</u> |
|---|---------------|--|---------------|
| Defense Documentation Center<br>Cameron Station<br>Alexandria, VA 22314   | 12            | Naval Air Propulsion Test Center<br>Trenton, NJ 08628<br>ATTN: Library   | 1             |
| Office of Naval Research<br>Department of the Navy<br>800 N. Quincy Street<br>Arlington, VA 22217                                   |               | Naval Construction Battalion<br>Civil Engineering Laboratory<br>Port Hueneme, CA 93043<br>ATTN: Materials Division     | 1             |
| ATTN: Code 471  | 1             | Naval Electronics Laboratory<br>San Diego, CA 92152<br>ATTN: Electron Materials<br>Science Division                    | 1             |
| Code 102  | 1             |  |               |
| Code 470  | 1             |  |               |
| Commanding Officer<br>Office of Naval Research<br>Branch Office<br>Building 114, Section D<br>666 Summer Street<br>Boston, MA 02210 | 1             | Naval Missile Center<br>Materials Consultant<br>Code 3312-1<br>Point Mugu, CA 92041                                    | 1             |
| Commanding Officer<br>Office of Naval Research<br>Branch Office<br>536 South Clark Street<br>Chicago, IL 60605                      | 1             | Commanding Officer<br>Naval Surface Weapons Center<br>White Oak Laboratory<br>Silver Spring, MD 20910<br>ATTN: Library | 1             |
| Naval Research Laboratory<br>Washington DC 20375  |               | David W. Taylor Naval Ship<br>Research and Development center<br>Materials Department<br>Annapolis, MD 21402           | 1             |
| Attn: Codes 6000  | 1             |  |               |
| 6100  | 1             | Naval Undersea Center<br>San Diego, CA 92132<br>ATTN: Library  | 1             |
| 6300  | 1             |  |               |
| 6400  | 1             |  |               |
| 2627  |               | Naval Underwater System Center<br>Newport, RI 02840<br>ATTN: Library   | 1             |
| Naval Air Development Center<br>Code 302<br>Warminster, PA 18964<br>ATTN: Mr. F.S. Williams   | 1             | Naval Weapons Center<br>China Lake, CA 93555<br>ATTN: Library  | 1             |
| Naval Postgraduate School<br>Monterey, CA 93840<br>ATTN: Mechanical Engineering<br>Department                                       | 1             |  |               |

# BASIC DISTRIBUTION LIST (Continued)

| <u>Organization</u>   | <u>Copies</u> | <u>Organization</u>  | <u>Copies</u> |
|---|---------------|--|---------------|
| Naval Air Systems Command<br>Washington, DC 20360<br>ATTN: Codes 52031<br>52032   | 1             | NASA Headquarters<br>Washington, DC 20546<br>ATTN: Code RRM  | 1             |
| Naval Sea System Command<br>Washington, DC 20362<br>ATTN: Code 035  | 1             | NASA (216) 433-4000<br>Lewis Research Center<br>21000 Brookpark Road<br>Cleveland, OH 44135<br>ATTN: Library                       | 1             |
| Naval Facilities<br>Engineering Command<br>Alexandria, VA 22331<br>ATTN: Code 03  | 1             | National Bureau of Standards<br>Washington, DC 20234<br>ATTN: Metallurgy Division<br>Inorganic Materials Division                  | 1<br>1        |
| Scientific Advisor<br>Commandant of the Marine Corps<br>Washington, DC 20380<br>ATTN: Code AX   | 1             | Director Applied Physics Laboratory<br>University of Washington<br>1013 Northeast Fortieth Street<br>Seattle, WA 98105             | 1             |
| Naval Ship Engineering Center<br>Department of the Navy<br>Washington, DC 20360<br>ATTN: Code 6101  | 1             | Defense Metals and Ceramics<br>Information Center<br>Battelle Memorial Institute<br>505 King Avenue<br>Columbus, OH 43201          | 1             |
| Army Research Office<br>P.O. Box 12211<br>Triangle Part, NC 27709<br>ATTN: Metallurgy and<br>Ceramics Program   | 1             | Metals and Ceramics Division<br>Oak Ridge National Laboratory<br>P.O. Box X<br>Oak Ridge, TN 37380                                 | 1             |
| Army Materials and Mechanics<br>Research Center<br>Watertown, MA 02172<br>ATTN: Research Programs Office  | 1             | Los Alamos Scientific Laboratory<br>P.O. Box 1663<br>Los Alamos, NM 87544<br>ATTN: Report Librarian                                | 1             |
| Air Force Office of<br>Scientific Research<br>Bldg. 410<br>Bolling Air Force Base<br>Washington, DC 20332<br>ATTN: Chemical Science<br>Directorate<br>Electronics & Solid State<br>Sciences Directorate | 1<br>1        | Argonne National Laboratory<br>Metallurgy Division<br>P.O. Box 229<br>Lemont, IL 60439   | 1             |
| Air Force Materials Laboratory<br>Wright-Patterson AFB<br>Dayton, OH 45433  | 1             | Brookhaven National Laboratory<br>Technical Information Division<br>Upton, Long Island<br>New York 11973<br>ATTN: Research Library | 1             |

BASIC DISTRIBUTION LIST (Continued)

| <u>Organization</u>           | <u>Copies</u> | <u>Organization</u>      | <u>Copies</u> |
|-------------------------------|---------------|--------------------------|---------------|
| Library                       |               | Office of Naval Research |               |
| Building 50, Room 134         |               | Branch Office            |               |
| Lawrence Radiation Laboratory |               | 1030 East Green Street   |               |
| Berkeley, CA                  | 1             | Pasadena, CA 91106       | 1             |

## SUPPLEMENTARY DISTRIBUTION LIST

### Technical and Summary Reports

Professor Albert E. Miller  
University of Notre Dame  
Box 8  
Notre Dame, IN 46556

Professor Karl J. Strnat  
University of Dayton  
Magnetic Laboratory  
Dayton, OH 45469

Dr. J.J. Becker  
General Electric Research  
and Development Center  
P.O. Box 8  
Schenectady, NY 12301

Professor W.E. Wallace  
Department of Chemistry  
University of Pittsburgh  
Pittsburgh, PA 15213

Dr. Richard P. Allen  
Battelle-Northwest  
Richland, WA 99352

Dr. Howard T. Savage  
Naval Surface Weapons Center  
White Oak  
Silver Spring, MD 20910

Mr. Harold Garrett  
Air Force Materials Laboratory  
LTE, Bldg. 16  
Wright-Patterson Air Force Base  
Dayton, OH 45433

Dr. L.D. Jennings  
Army Materials and Mechanics  
Research Center  
Watertown, MA 02172

Dr. J.O. Dimmock, Director  
Electronic and Solid State  
Sciences Program (Code 427)  
Office of Naval Research  
Arlington, VA 22217

Assistant Chief for Technology  
(Code 2000)  
Office of Naval Research  
Arlington, VA 22217

Strategic Systems Projects Office  
Department of the Navy  
Washington, DC

Professor G.S. Ansell  
Rensselaer Polytechnic Institute  
Dept. of Metallurgical Engineering  
Troy, NY 12181

Dr. David L. Martin  
General Electric Research  
and Development Center  
P.O. Box 8  
Schenectady, NY 12301

Professor M. Cohen  
Massachusetts Institute of Technology  
Department of Metallurgy  
Cambridge, MA 02139

Professor J.W. Morris, Jr.  
University of California  
College of Engineering  
Berkeley, CA 94720

Professor O.D. Sherby  
Stanford University  
Materials Sciences Division  
Stanford, CA 94300

SUPPLEMENTARY DISTRIBUTION LIST (Continued)

Dr. E.A. Starke, Jr.  
Georgia Institute of Technology  
School of Chemical Engineering  
Atlanta, GA 30332

Professor David Turnbull  
Harvard University  
Division of Engineering and  
Applied Physics  
Cambridge, MA 02139

Dr. D.P.H. Hasselman  
Montana Energy and MHD Research  
and Development Institute  
P.O. Box 3809  
Butte, MT 59701

Dr. L. Hench  
University of Florida  
Ceramics Division  
Gainesville, FL 32601

Dr. J. Ritter  
University of Massachusetts  
Department of Mechanical  
Engineering  
Amherst, MA 01002

Professor J.B. Cohen  
Northwestern University  
Dept. of Material Sciences  
Evanston, IL 60201

Director  
Materials Sciences  
Defense Advanced Research  
Projects Agency  
1400 Wilson Boulevard  
Arlington, VA 22209

Professor H. Conrad  
University of Kentucky  
Materials Department  
Lexington, KY 40506

Dr. A.G. Evans  
Dept. of Material Sciences  
and Engineering  
University of California  
Berkeley, CA 94720

Professor H. Herman  
State University of New York  
Material Sciences Division  
Stony Brook, NY 11794

Professor J.P. Hirth  
Ohio State University  
Metallurgical Engineering  
Columbus, OH 43210

Professor R.M. Latanision  
Massachusetts Institute of Technology  
77 Massachusetts Avenue  
Room E19-702  
Cambridge, MA 02139

Dr. Jeff Perkins  
Naval Postgraduate School  
Monterey, CA 93940

Dr. R.P. Wei  
Lehigh University  
Institute for Fracture and  
Solid Mechanics  
Bethlehem, PA 18015

Professor G. Sines  
University of California  
at Los Angeles  
Los Angeles, CA 90024

Professor H.G.F. Wilsdorf  
University of Virginia  
Department of Materials Science  
Charlottesville, VA 22903

Dr. A. Tauber  
Dept. of the Army  
HQ, U.S. Army Electronic Command  
Fort Monmouth, NY 07703

SUPPLEMENTARY DISTRIBUTION LIST (Continued)

Mr. K.K. Jin  
Strategic Systems Division  
Autonetics Group  
3370 Miraloma Avenue  
P.O. Box 4192  
Anaheim, CA 92803

Mr. N. Horowitz  
The Aerospace Corporation  
2350 East El Segundo Boulevard  
El Segundo, CA

Mr. Francis W. Wessbecher  
Unit Head  
Inertial Component Engineering  
Singer Kearfott Division  
150 Totowa Road  
Wayne, NJ 07470

National Magnet Laboratory  
Massachusetts Institute of Technology  
145 Albany Street  
Cambridge, MA 02139  
ATTN: Dr. Donald T. Stevenson (2)  
Assistant Director

Mr. Carl Flom  
Delco Electronics  
7929 South Howell  
Box 471  
Milwaukee, WI 53201

David Schwab  
Air Research Mfg. Co.  
2525 W. 190th Street  
Torrance, CA 90209

DATE  
ILME  
—8